© 2020. Published by The Company of Biologists Ltd | Journal of Cell Science (2020) 133, jcs236877. doi:10.1242/jcs.236877

RESEARCH ARTICLE

Multivalent nephrin–Nck interactions define a threshold for clustering and tyrosine-dependent nephrin endocytosis

Claire E. Martin[1], Laura A. New[1], Noah J. Phippen[1], Ava Keyvani Chahi[1], Alexander E. Mitro[1], Tomoko Takano[2], Tony Pawson[3,4,‡], Ivan M. Blasutig[3,4,*] and Nina Jones[1,§]

ABSTRACT

Assembly of signaling molecules into micrometer-sized clusters is driven by multivalent protein-protein interactions, such as those found within the nephrin–Nck (Nck1 or Nck2) complex. Phosphorylation on multiple tyrosine residues within the tail of the nephrin transmembrane receptor induces recruitment of the cytoplasmic adaptor protein Nck, which binds via its triple SH3 domains to various effectors, leading to actin assembly. The physiological consequences of nephrin clustering are not well understood. Here, we demonstrate that nephrin phosphorylation regulates the formation of membrane clusters in podocytes. We also reveal a connection between clustering and endocytosis, which appears to be driven by threshold levels of nephrin tyrosine phosphorylation and Nck SH3 domain signaling. Finally, we expose an *in vivo* correlation between transient changes in nephrin tyrosine phosphorylation, nephrin localization and integrity of the glomerular filtration barrier during podocyte injury. Altogether, our results suggest that nephrin phosphorylation determines the composition of effector proteins within clusters to dynamically regulate nephrin turnover and podocyte health.

KEY WORDS: Podocyte, Nephrin, Phosphotyrosine, Nck, Dynamin, Clustering

INTRODUCTION

Organization of plasma membrane signaling proteins into higher-order assemblies or clusters is essential to control cellular responses to external cues (Mayer and Yu, 2018). Phase separation has recently emerged as a mechanism of membrane protein clustering, and it is driven by interactions between multivalent proteins, such as those found within the nephrin–Nck–N-WASp complex (herein, Nck refers to both Nck1 and Nck2 except where specified; N-WASp is also known as WASL) (Mayer and Yu, 2018). Nephrin is a transmembrane adhesion molecule that contains three phosphorylated YDxV motifs on its intracellular tail, each of which can bind the SH2 domain of the Nck1 and Nck2 (Nck1/2) cytoplasmic adaptors (Jones et al., 2006). Nck proteins also contain three SH3 domains and they associate with multiple proline-rich motifs (PRMs) on N-WASp (Rohatgi et al., 2001), which in turn binds and activates the Arp2/3 complex to promote actin nucleation (Svitkina and Borisy, 1999). The componentry of nephrin–Nck and Nck–N-WASp signaling has been studied using synthetic reconstitution systems, wherein the valency of nephrin YDxV motifs, Nck SH3 domains and N-WASp PRMs correlates with phase separation and actin assembly in solution (Banjade and Rosen, 2014; Ditlev et al., 2012; Li et al., 2012). Moreover, recent studies have shown that the highly cross-linked nature of the nephrin–Nck–N-WASp complex increases the dwell time and specific activity of N-WASp and Arp2/3, further driving actin polymerization at sites of phase-separated clusters (Case et al., 2019). These findings support the notion that nephrin–Nck–N-WASp clustering leads to the formation of a distinct actin-associated signaling node, yet the functional implications of these multivalent interactions in a relevant physiological setting have yet to be revealed.

Nephrin serves as the principal component of the slit diaphragm, a unique intercellular junction bridging the foot processes that extend from adjacent podocytes in the kidney (Scott and Quaggin, 2015). At the cell surface, *trans* interactions between extracellular immunoglobulin domains of nephrin form the core of the slit diaphragm, allowing it to act as a size-selective blood filtration barrier (Fig. 1A). Inside the cell, nephrin functions as a signaling scaffold to bind proteins such as Nck (New et al., 2014), which are crucial for supporting the podocyte's specialized morphology (Jones et al., 2006, 2009). Mutation of all three YDxV motifs (hereafter referred to as the nephrin-Y3F mutation) disrupts interaction with Nck and its ability to induce actin assembly at nephrin clusters in fibroblasts (Blasutig et al., 2008; Jones et al., 2006). Furthermore, changes in YDxV phosphorylation are observed in human kidney diseases and related experimental models in rodents (Jones et al., 2006; Uchida et al., 2008), and mice harboring the nephrin-Y3F knock-in mutation develop filtration defects with age (New et al., 2016). Precise regulation of nephrin–Nck signaling is therefore a central determinant of podocyte health.

Nephrin mislocalization is commonly observed in kidney diseases of hereditary and acquired origins (Königshausen et al., 2016; Martin et al., 2018; Nishibori et al., 2004; Ohashi et al., 2010; Shimizu et al., 2002; Soda et al., 2012; Wernerson et al., 2003), suggesting that abnormal nephrin trafficking likely contributes to barrier dysfunction. Localization of nephrin within the slit diaphragm requires dynamic phosphorylation events and endocytic recycling (Soda and Ishibe, 2013), though the molecular mechanisms that control this interplay are not well understood. Along with Nck, several slit diaphragm-associated signaling proteins implicated in endocytosis, including N-WASp and the GTPase dynamin, which participates in vesicle scission (Ferguson and De Camilli, 2012), are essential to maintain podocyte structure (Jones et al., 2009; Schell et al., 2013; Soda et al.,

[1]Department of Molecular and Cellular Biology, University of Guelph, Guelph, ON, N1G 2W1, Canada. [2]Department of Medicine, McGill University Health Centre, Montreal, QC, H4A 3J1, Canada. [3]Lunenfeld-Tanenbaum Research Institute, Mount Sinai Hospital, Toronto, Ontario, M5G 1X5, Canada. [4]Department of Molecular Genetics, University of Toronto, Toronto, Ontario, M5S 1A8, Canada. *Present address: Department of Pathology and Laboratory Medicine, University of Ottawa, Ottawa, ON, K1N 6N5, Canada.
‡Deceased

§Author for correspondence (jonesmcb@uoguelph.ca)

N.J., 0000-0003-2786-2404

Received 23 July 2019; Accepted 10 January 2020

Journal of Cell Science (2020) 133, jcs236877. doi:10.1242/jcs.236877

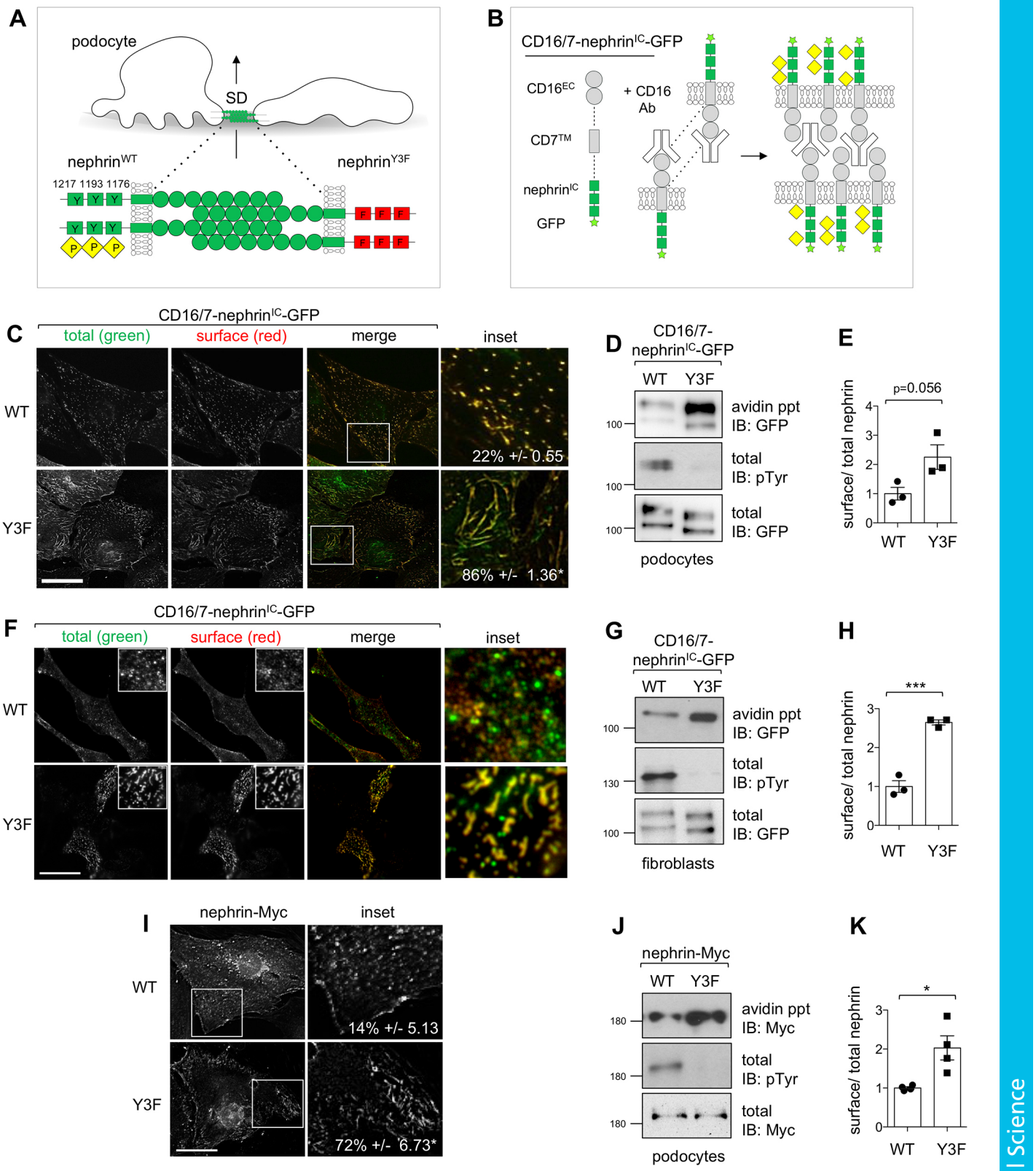

Fig. 1. See next page for legend.

2012). Moreover, dynamin-deficient podocytes show reduced nephrin internalization and an accumulation of arrested endocytic pits, which contain Arp2/3, alluding to a connection between the endocytosis machinery and the actin cytoskeleton in these cells (Soda et al., 2012). Intriguingly, emerging evidence suggests that phase separation can drive membrane invagination and endocytosis in several cell types (Hilgemann et al., 2020). In this article, we now establish a connection between clustering and endocytosis in

Journal of Cell Science (2020) 133, jcs236877. doi:10.1242/jcs.236877

Fig. 1. Nephrin YDxV motifs are required for its clustering and endocytosis in podocytes. (A) Schematic of the podocyte slit diaphragm (SD) formed by nephrin Ig domains (green). Phosphorylation (yellow) on three intracellular YDxV motifs (human numbering system) regulates podocyte morphology, and Y-to-F mutations (red) in these three motifs (creating the nephrin-Y3F mutation) lead to progressive loss of podocyte shape and SD function. (B) The CD16/7-nephrin fusion protein, which consists of the extracellular (EC) region of CD16, the transmembrane (TM) region of CD7, the intracellular (IC) region of nephrin, and GFP (star), allows for CD16 antibody-mediated clustering and phosphorylation of nephrin tyrosines. (C) Total (green; post-permeabilization) and surface (red; pre-permeabilization) nephrin labeling of cultured mouse podocytes (MPCs) transduced with CD16/7-nephrin^{IC}-GFP adenoviruses expressing either wild-type nephrin (WT) or nephrin-Y3F and stimulated with CD16 antibodies for 30 min show the punctate versus loose aggregates of nephrin, respectively. The percentage of cells with a predominance of elongated clusters is indicated. (D) Transduced MPCs were subjected to surface biotinylation, followed by lysis, streptavidin agarose precipitation (ppt) and immunoblotting (IB) as indicated. A portion of the initial lysate was saved to represent the total protein. (E) Densitometric quantification of surface/total nephrin from D. Y3F values are expressed relative to WT (n=3). (F) Total (green) and surface (red) nephrin labeling of mouse embryonic fibroblasts (MEFs) expressing CD16/7-nephrin(WT)^{IC}-GFP or CD16/7-nephrin(Y3F)^{IC}-GFP and stimulated with CD16 antibodies for 30 min. (G,H) Surface biotinylation and densitometric quantification in MEFs expressing CD16/7-nephrin^{IC}-GFP (n=3) shows increased surface expression of nephrin-Y3F compared with WT. (I) Total nephrin labeling of MPCs transduced with adenoviruses expressing full-length Myc-tagged WT or Y3F nephrin. The percentage of cells with elongated clusters is indicated. (J,K) Surface biotinylation and densitometric quantification in MPCs transduced with full-length WT or Y3F nephrin (n=3). Boxed areas in image panels indicate the region shown in insets. Scale bars: 20 µm. *P<0.05, ***P<0.001 by two-tailed t-test for normally distributed data (E,H) or Mann–Whitney test for non-parametric data sets (K).

podocytes *in vitro* and *in vivo*, which appears to be regulated by threshold levels of nephrin tyrosine phosphorylation and Nck SH3 domain signaling with N-WASp and dynamin. We also show that a transient rise in nephrin phosphorylation occurs upon podocyte injury and correlates with decreased surface nephrin, leading to filtration barrier leakage, and that mice lacking the Nck-binding sites on nephrin are resistant to this injury. Altogether, our data suggest that nephrin–Nck interactions provide a tunable system to regulate protein composition and membrane turnover at the slit diaphragm.

RESULTS

Nephrin YDxV phosphorylation regulates nephrin clustering and surface expression in podocytes

To probe the downstream consequences of nephrin–Nck clustering in podocytes, we first monitored the subcellular distribution of nephrin and the Y3F variant, which harbors Y-to-F substitutions in all three of the Nck-binding YDxV motifs to prevent their phosphorylation (Fig. 1A). To facilitate these studies in cultured podocytes, which lack robust expression of endogenous nephrin, we generated a series of adenoviruses containing full-length Myc-tagged wild-type (WT) or Y3F nephrin, or chimeric nephrin proteins in which the intracellular (IC) regions of GFP-tagged WT or Y3F nephrin are fused to the extracellular domain of CD16 (FCGR3A) and the transmembrane domain of CD7 (denoted CD16/7) (Fig. 1B). We and others have previously reported that clustering of CD16/7-nephrin(WT)^{IC} is induced upon addition of anti-CD16 cross-linking antibodies, that the clusters persist for several hours, and that this chimera is a suitable surrogate for full-length nephrin in signaling assays (Blasutig et al., 2008; Jones et al., 2006; Verma et al., 2003). Similar to findings in mouse embryonic fibroblasts (MEFs) (Blasutig et al., 2008; Jones et al., 2006; Verma et al., 2003), cross-linking of CD16/7-nephrin(WT)^{IC} in mouse podocytes with CD16 antibodies for 30 min induced the formation of punctate clusters throughout the cell (Fig. 1C, left). Intriguingly, CD16/7-nephrin(Y3F)^{IC} organization within podocytes was heterogeneous, displaying clusters of varying sizes, with a predominance of clusters with an elongated morphology (Fig. 1C, left). To investigate the localization of these structures, we performed surface immunolabeling of nephrin in podocytes expressing CD16/7-nephrin^{IC}-GFP, in which total nephrin was labeled with green and surface nephrin was labeled with red. Under these conditions, CD16/7-nephrin(WT)^{IC} clusters appear as both green and yellow in the merged panel (Fig. 1C, center and right), indicating that they are found both in the cytosol and on the cell surface, as previously reported (Blasutig et al., 2008; Qin et al., 2009). The clusters that accumulate with the CD16/7-nephrin(Y3F)^{IC} protein also appear with both total (green) and surface (red) labeling (yellow in merge) (Fig. 1C, center and right). However, quantification of these structures revealed that over 86% of CD16/7-nephrin(Y3F)^{IC}-expressing cells contained elongated clusters, compared with 22% of CD16/7-nephrin(WT)^{IC}-expressing cells (Fig. 1C). We further examined the membrane expression profiles of the CD16/7-nephrin(WT)^{IC} or CD16/7-nephrin(Y3F)^{IC} proteins in transduced podocytes using cell surface biotinylation assays. Consistent with our imaging observations, CD16/7-nephrin(Y3F)^{IC} is enriched over 2-fold on the cell surface compared with CD16/7-nephrin(WT)^{IC} (Fig. 1D,E). To ensure that formation of these structures was intrinsic to nephrin, we repeated these experiments in MEFs, and again observed the appearance of elongated clusters coincident with an increase in surface nephrin accumulation with CD16/7-nephrin(Y3F)^{IC} (Fig. 1F-H). In addition, we transduced the corresponding full-length nephrin constructs into podocytes, and likewise noted the induction of elongated clusters and heightened surface levels of nephrin-Y3F compared with nephrin-WT (Fig. 1I-K). Biotinylation assays on HEK cells expressing full-length nephrin showed similar results (Fig. S1A,B). Lastly, to verify the link between nephrin tyrosine phosphorylation and surface dynamics, we expressed full-length nephrin-WT and nephrin-Y3F with and without active Fyn kinase in HEK cells and performed surface biotinylation assays. We found that Fyn induced a decrease in surface levels of nephrin and that this induction was significantly greater for nephrin-WT compared with nephrin-Y3F, supporting a role for these particular tyrosines in nephrin endocytosis (Fig. S1C,D). Altogether, our results implicate nephrin phosphorylation on the Nck-binding sites in regulating cluster formation and nephrin surface expression in podocytes.

Genetic loss of nephrin YDxV phospho-sites impairs nephrin localization *in vivo*

To complement our *in vitro* findings, we next monitored nephrin localization in our gene-targeted nephrin-Y3F mice, which develop progressive proteinuria and podocyte dysmorphology as they age (New et al., 2016). Compared with WT control animals, aged nephrin-Y3F mice show mislocalization of nephrin along with its binding partner podocin in immunostained glomerular tissue sections, with both proteins present in focal aggregates (Fig. 2A). To examine this in greater detail, we utilized super-resolution structured illumination microscopy (SR-SIM) to image nephrin-immunostained kidney sections prepared from WT and Y3F mice. Again we observed aggregates of nephrin in Y3F mice, whereas nephrin showed fine linear staining along the capillary wall in WT mice (Fig. 2B). Lastly, *ex vivo* biotinylation of intact glomeruli isolated from kidneys of WT and mutant animals revealed a significant 2-fold increase in surface nephrin levels in nephrin-Y3F mice compared with WT controls (Fig. 2C,D). Altogether, these

Journal of Cell Science (2020) 133, jcs236877. doi:10.1242/jcs.236877

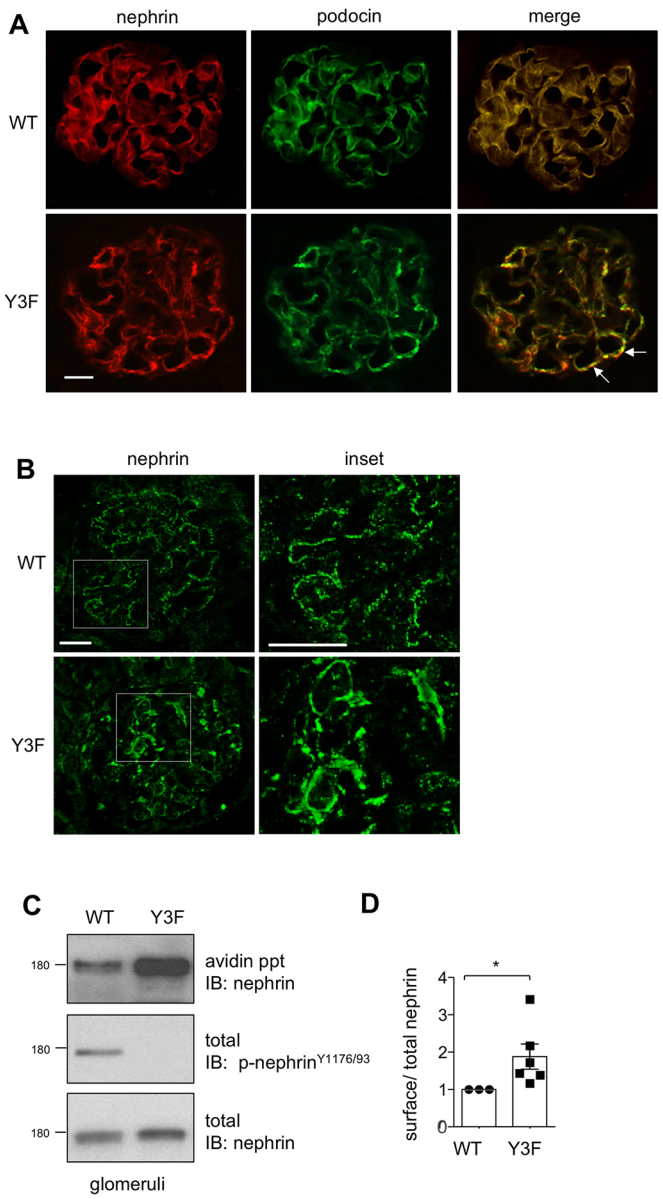

Fig. 2. Genetic disruption of nephrin YDxV motifs perturbs nephrin localization *in vivo*. (A) Nephrin (red) and podocin (green) immunostaining of kidney sections from 6-month-old WT and nephrin-Y3F mice on CD-1 background shows abnormal aggregation of both proteins in glomeruli of mutant mice (arrows in merged image). Scale bar: 10 µm. (B) Super-resolution structured illumination microscopy imaging of nephrin localization in glomeruli from the mice shown in A. Boxed areas indicate the region shown in insets. Scale bars: 10 µm. (C) Glomeruli from 6- to 9-month-old CD-1 WT or Y3F mice were isolated and subjected to surface biotinylation, followed by lysis, streptavidin agarose precipitation (ppt) and immunoblotting (IB) as indicated. A portion of the initial lysate was saved to represent the total protein. (D) Densitometric quantification of surface/total nephrin from C. Y3F values are expressed relative to WT (n=6/Y3F, n=3/WT). *P<0.05 by one-sample t-test.

results support the notion that loss of nephrin phosphorylation on the YDxV motifs impairs nephrin localization in podocytes.

Recruitment of the endocytic mediator clathrin is dependent on YDxV phospho-sites

Previous studies have shown that phosphorylation of nephrin triggers its internalization into endosomal compartments using both clathrin-dependent and -independent mechanisms (Jeon et al., 2012; Lahdenperä et al., 2003; Qin et al., 2009). To investigate whether nephrin clusters represent endocytic structures, we first examined our well-characterized fibroblast model for the presence of nephrin and clathrin at clusters formed after 30 min of CD16 antibody treatment in cells expressing CD16/7-nephrin(WT)^{IC} or CD16/7-nephrin(Y3F)^{IC} (Fig. 3A,B). We observed nephrin and clathrin in close proximity in most of the clusters in CD16/7-nephrin(WT)^{IC} cells (Fig. 3A, arrows). Interestingly, in CD16/7-nephrin(Y3F)^{IC} cells, clathrin was also localized to clusters but only observed close to the tips of the elongated clusters rather than along the entire structure (Fig. 3B, arrows). Next, we performed a time-course analysis of CD16/7-nephrin(WT)^{IC} cluster formation and surface expression in mouse podocytes, and also monitored nephrin colocalization with clathrin (Fig. 3C-E). In line with our previous kinetic analysis in MEFs (Blasutig et al., 2008), confocal imaging revealed surface cluster formation of nephrin-WT within 15 min of the addition of CD16 antibodies, some of which colocalized with clathrin (Fig. 3D, arrow), demonstrating that endocytic machinery is recruited to nephrin signaling clusters. At 30 min, colocalization between nephrin-WT and clathrin continued to be detected; however, the nephrin-clathrin clusters were mostly cytosolic (Fig. 3E, arrow). Lastly, we examined clathrin co-staining in podocytes expressing the CD16/7-nephrin(Y3F)^{IC} mutant after 30 min of CD16 antibody clustering (Fig. 3F). Surface nephrin-Y3F clusters also shared some localization with clathrin, but only at the termini of the elongated clusters (Fig. 3F, arrow). Altogether, our results support the conclusion that the elongated clusters seen with nephrin-Y3F represent nephrin-enriched endocytic structures.

Multisite nephrin phosphorylation provides a threshold for cluster assembly

The three nephrin YDxV motifs are arranged in tandem and our previous studies have shown that a single YDxV motif is sufficient to recruit Nck and promote actin assembly (Blasutig et al., 2008; New et al., 2013; Verma et al., 2003), suggesting that they might be functionally redundant. To determine the relative contributions of each YDxV motif in cluster assembly, we expressed chimeric nephrin proteins with Y-to-F point mutations in one, two or all three YDxV motifs (Fig. 4A) alongside CD16/7-nephrin(WT)^{IC} in MEFs, performed CD16 antibody cross-linking for 30 min, and monitored nephrin distribution by surface immunolabeling. Unexpectedly, we noted that disruption of a single YDxV motif caused elongated clusters to amass (Y1F series), and this phenotype was enhanced when any two motifs were mutated (Y2F series) (Fig. 4A). Quantification of the percentage of elongated clusters revealed that all mutants were significantly different from WT (Fig. 4B). Notably, a gradient or dose-dependent effect existed between Y1F single mutants with all Y2F double mutants, and between all Y2F mutants and the triple Y3F mutant (Fig. 4B). Interestingly, of the single mutants, Y1217F (denoted YYF) induced more elongated clusters than either Y1176F (denoted FYY) or Y1193F (denoted YFY) (Fig. 4B), which may reflect its preferential binding to Nck (Jones et al., 2006). Collectively, our findings suggest that the efficiency of nephrin clustering correlates with the number of nephrin YDxV-based phosphorylation sites.

Nephrin clustering and endocytosis are dependent on the recruitment of actin via Nck SH3 domains

The ability of Nck to associate with all YDxV motifs and its central role in actin assembly prompted us to explore the consequence of Nck disruption on nephrin clustering and surface localization. To

Journal of Cell Science (2020) 133, jcs236877. doi:10.1242/jcs.236877

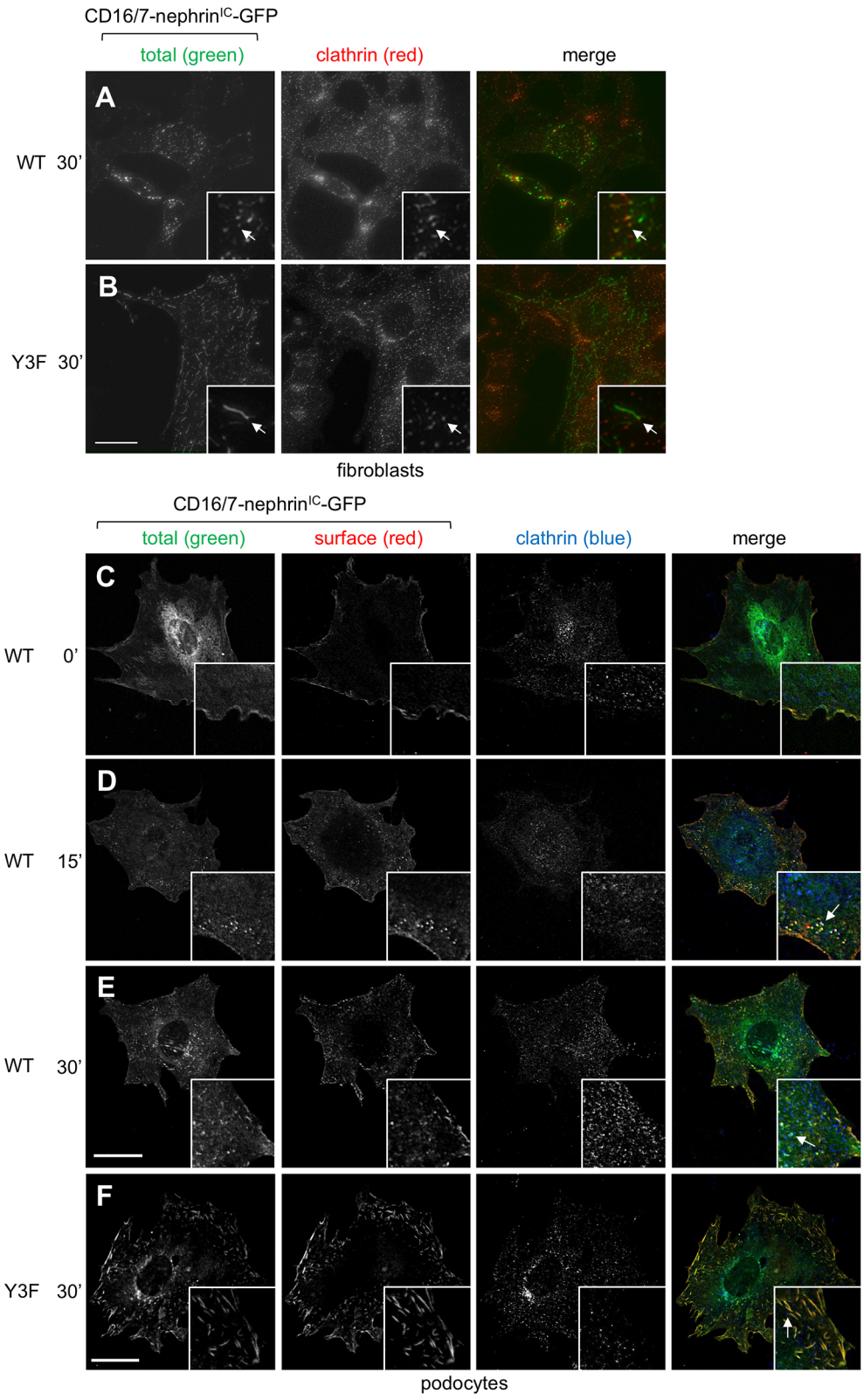

Fig. 3. Dynamics of CD16/7-nephrin^{IC}-GFP clustering and endocytosis. (A,B) CD16 nephrin (green) and clathrin (red) labeling of MEFs transfected with the indicated CD16/7-nephrin^{IC}-GFP constructs and stimulated for 30 min with CD16. In nephrin-WT cells, nephrin and clathrin are together in most clusters (A, arrows), whereas in nephrin-Y3F cells, clathrin is only observed close to the tips of the elongated clusters (B, arrows). (C-E) Total CD16 nephrin (green; post-permeabilization), surface CD16 nephrin (red; pre-permeabilization) and clathrin (blue) labeling of MPCs transduced with CD16/7-nephrin(WT)^{IC}-GFP and stimulated with CD16 antibody for the indicated times. Surface nephrin-WT clusters colocalized with clathrin can be observed at 15 min post-clustering (D, arrow). At 30 min, the majority of nephrin-WT colocalized with clathrin can be found in internalized clusters (E, arrow). (F) Comparison of CD16/7-nephrin(Y3F)^{IC}-GFP after 30 min of CD16 clustering. At this time, surface elongated clusters predominate with nephrin-Y3F, which only partially colocalize with clathrin (F, arrow). Scale bars: 20 µm.

interfere with Nck signaling specifically, we employed a FLAG-tagged Nck2 variant with point mutations in all three tandem SH3 domains (SH3*x3) to prevent binding to the proline-rich sequences of downstream effectors, including N-WASp (Fig. 5A). Nck2-SH3*x3 and Nck2-WT were co-transfected with GFP-tagged CD16/7-nephrin(WT)^{IC} into MEFs lacking Nck1/2 expression. Following addition of CD16 antibodies for 30 min to promote cross-linking, cells were fixed and permeabilized to allow immunolabeling of Nck2 (FLAG), as well as contrast-stained with Texas Red phalloidin to visualize F-actin. Expression of Nck2-WT stimulated development of discrete clusters containing colocalized nephrin and Nck, and they were associated with actin comet tails

Journal of Cell Science (2020) 133, jcs236877. doi:10.1242/jcs.236877

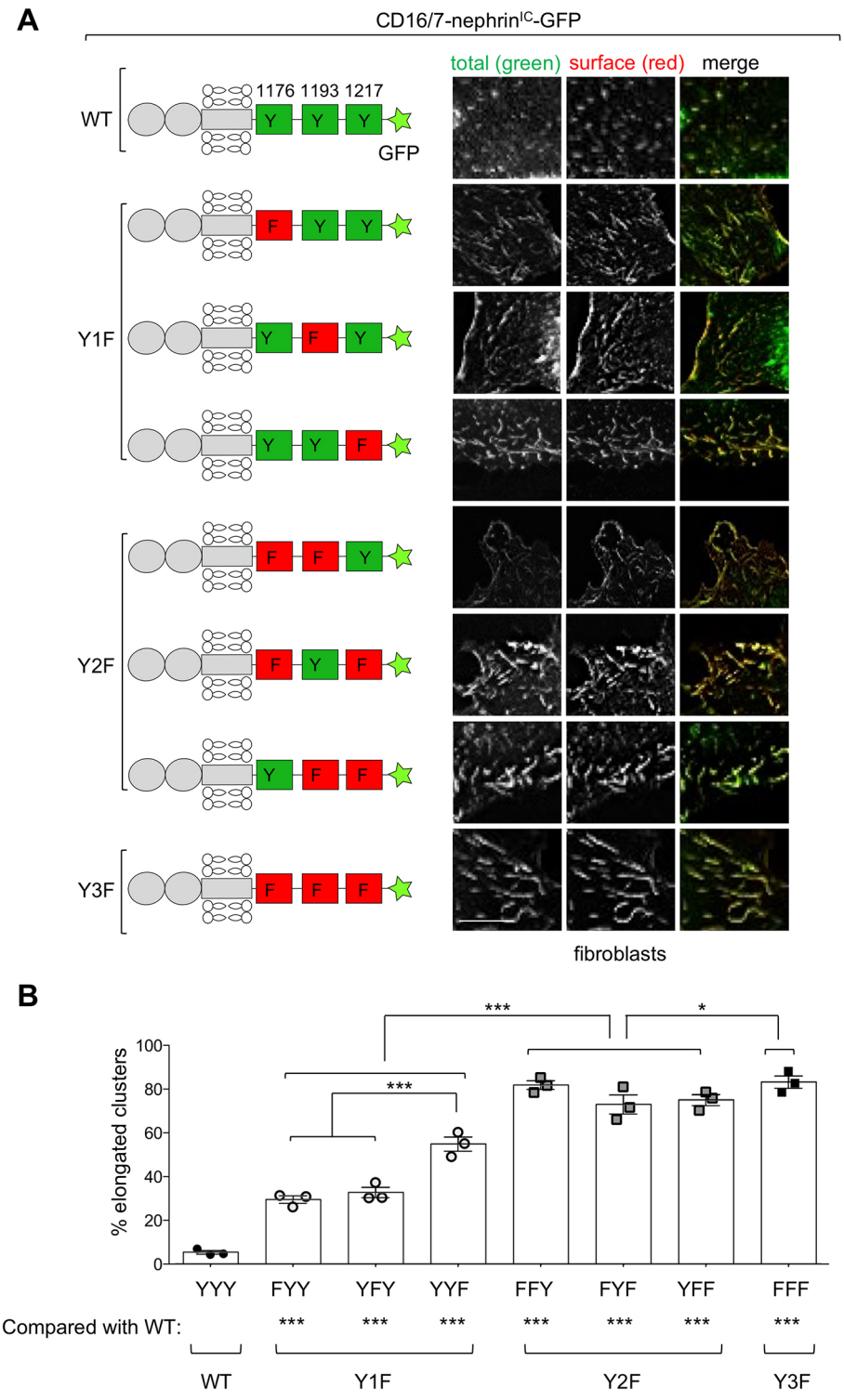

Fig. 4. Nephrin YDxV motif mutations scale with the defect in nephrin clustering. (A) Left: Schematics of the allelic series of CD16/7-nephrin^{IC}-GFP variants with one, two or three Y-to-F mutations in the three YDxV motifs (human numbering system). Right: Total (green; post-permeabilization) and surface (red; pre-permeabilization) nephrin labeling of MEFs transfected with WT, Y1F, Y2F or Y3F nephrin variants and stimulated with CD16 antibody. Scale bar: 20 µm. (B) Quantification of the percentage of cells in A with elongated clusters shows increased cluster formation with Y-to-F mutants, which amplified as the total number of YDxV mutations increased (n=3 for each). *P<0.05, ***P<0.001 by one-way ANOVA with post-hoc Tukey's HSD test.

(Fig. 5B, top panel), consistent with our previous findings (Jones et al., 2006). By contrast, Nck2-SH3*x3 maintained colocalization with nephrin, but both proteins showed a prominence of elongated clusters, similar to observations with nephrin Y-to-F mutations, and actin polymerization did not occur in the presence of the Nck mutant (Fig. 5B, middle panel, and 5C), in line with our previous findings (Blasutig et al., 2008). A similar defect was observed with Nck1-SH3*x3 but not Nck1-WT (Fig. S2). To examine further the nature of the elongated nephrin clusters associated with the Nck SH3*x3 mutants, we performed biotinylation assays in HEK cells transfected with full-length nephrin-WT. Co-expression of Nck2-WT but not Nck2-SH3*x3 caused a significant reduction in surface nephrin levels (Fig. 5D,E), and was correlated with a rise in nephrin phosphorylation (Fig. 5D). We have previously shown that Nck mediates recruitment of Fyn kinase (New et al., 2013), and indeed, expression of Fyn alone with nephrin-WT produced a similar effect on nephrin surface removal (Fig. S1C,D). Together, these studies suggest a link between nephrin cluster formation and

Journal of Cell Science (2020) 133, jcs236877. doi:10.1242/jcs.236877

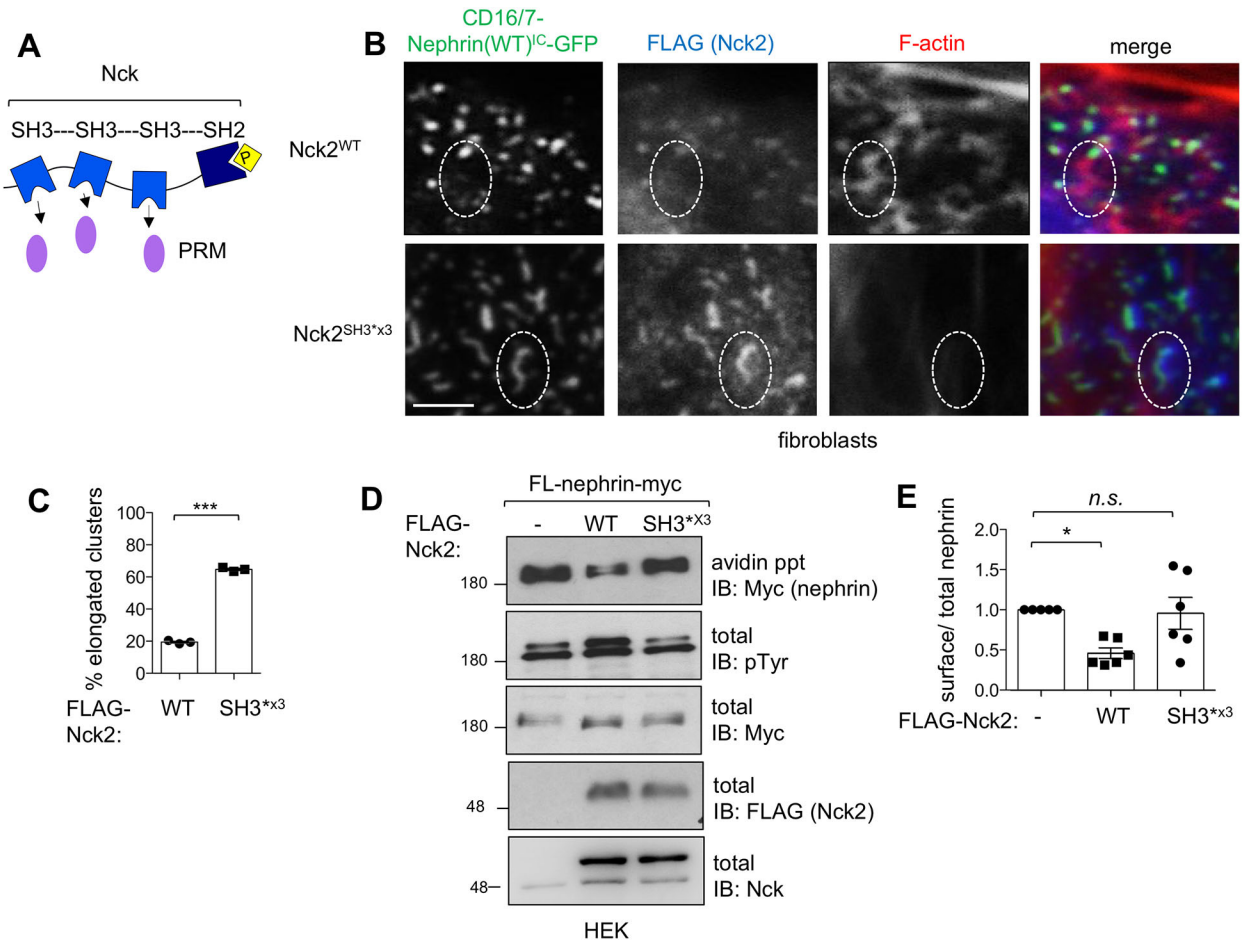

Fig. 5. Nephrin clustering and endocytosis are dependent on Nck-mediated downstream signaling. (A) Schematic of Nck showing three tandem SH3 domains, which engage proline-rich regions of downstream effectors, and the SH2 domain, which binds phosphorylated tyrosines (pY) on proteins such as nephrin. (B) Nck-null MEFs were co-transfected with CD16/7-nephrin(WT)^{IC}-GFP and FLAG-Nck2 variants, stimulated with CD16 antibody, and immunostained as indicated. Mutations in all three SH3 domains (SH3*x3) perturb F-actin polymerization (red) compared with WT, and disrupt clustering of both nephrin (green) and Nck2 (blue). Scale bar: 20 µm. Dashed oval indicates a nephrin cluster with an actin tail. (C) Quantification of the percentage of cells in B with elongated clusters (n=3 replicates for each). ***P<0.001 by one-way ANOVA with post-hoc Tukey's HSD test. (D) HEK293T cells transfected with full-length nephrin and Nck2 variants or nephrin alone were subjected to surface biotinylation, followed by lysis, streptavidin agarose precipitation (ppt) and immunoblotting (IB) as indicated. A portion of the initial lysate was saved to represent the total protein. (E) Densitometric quantification of surface/total nephrin from the data shown in D. Values are expressed relative to nephrin alone (left column) (n=5-6). *P<0.05 by Kruskal–Wallis test with post-hoc Dunn's Multiple Comparison test; n.s., not significant.

nephrin surface expression that is dependent on Nck SH3 domain signaling.

An engineered nephrin-Nck SH3 fusion protein restores nephrin clustering and endocytosis in the absence of YDxV phosphorylation

We next looked for a potential Nck binding partner with a known role in nephrin endocytosis. The protein dynamin-2 has been shown previously to influence nephrin's phospho-dependent trafficking in pancreatic beta cells through an unknown intermediate (Fornoni et al., 2010; Jeon et al., 2012), and it contains a proline-rich region required for vesicle scission (Ferguson et al., 2009). Given this potential connection, we investigated the ability of the Nck SH3 domains to bind dynamin-2. We initially determined that both Nck1 and Nck2 could associate with dynamin-2 upon co-expression in HEK cells (Fig. 6A). Notably, the strengths of these interactions were much weaker than those observed with N-WASp, suggesting that dynamin-2 may represent a low-affinity binding partner for Nck. Next, we verified that interaction of dynamin-2 with Nck2 requires intact SH3 but not SH2 domains (Fig. 6B), consistent with earlier reports using recombinant SH3 domains *in vitro* (Wunderlich et al., 1999). To confirm that dynamin-2 can alter surface nephrin levels, we co-expressed full-length nephrin-WT along with either dynamin2-WT or mutant dynamin2-K44A, a dominant negative unable to sever membranes (Ferguson and De Camilli, 2012) (Fig. S3A,B). We found that dynamin2-K44A co-expression resulted in a significant increase in surface nephrin levels, consistent with previous reports of reduced nephrin endocytosis when dynamin function is impaired (Lahdenperä et al., 2003; Qin et al., 2009).

Having identified a role for the Nck SH3 domains in nephrin clustering and localizing endocytic machinery to phosphorylated nephrin, we reasoned that transplantation of this region to the defective nephrin-Y3F protein should rewire the nephrin-Nck signal to bypass the YDxV motifs and allow for clustering and endocytosis to proceed. To this end, we generated a construct in which the three SH3 domains of Nck2 were cloned in-frame downstream of the intracellular tail of CD16/7-nephrin(Y3F)^{IC}, creating the CD16/7-nephrin(Y3F)^{IC}-Nck2(SH3x3)-GFP fusion protein (Fig. 6C) (Keyvani Chahi et al., 2016). We first confirmed that interaction

Journal of Cell Science (2020) 133, jcs236877. doi:10.1242/jcs.236877

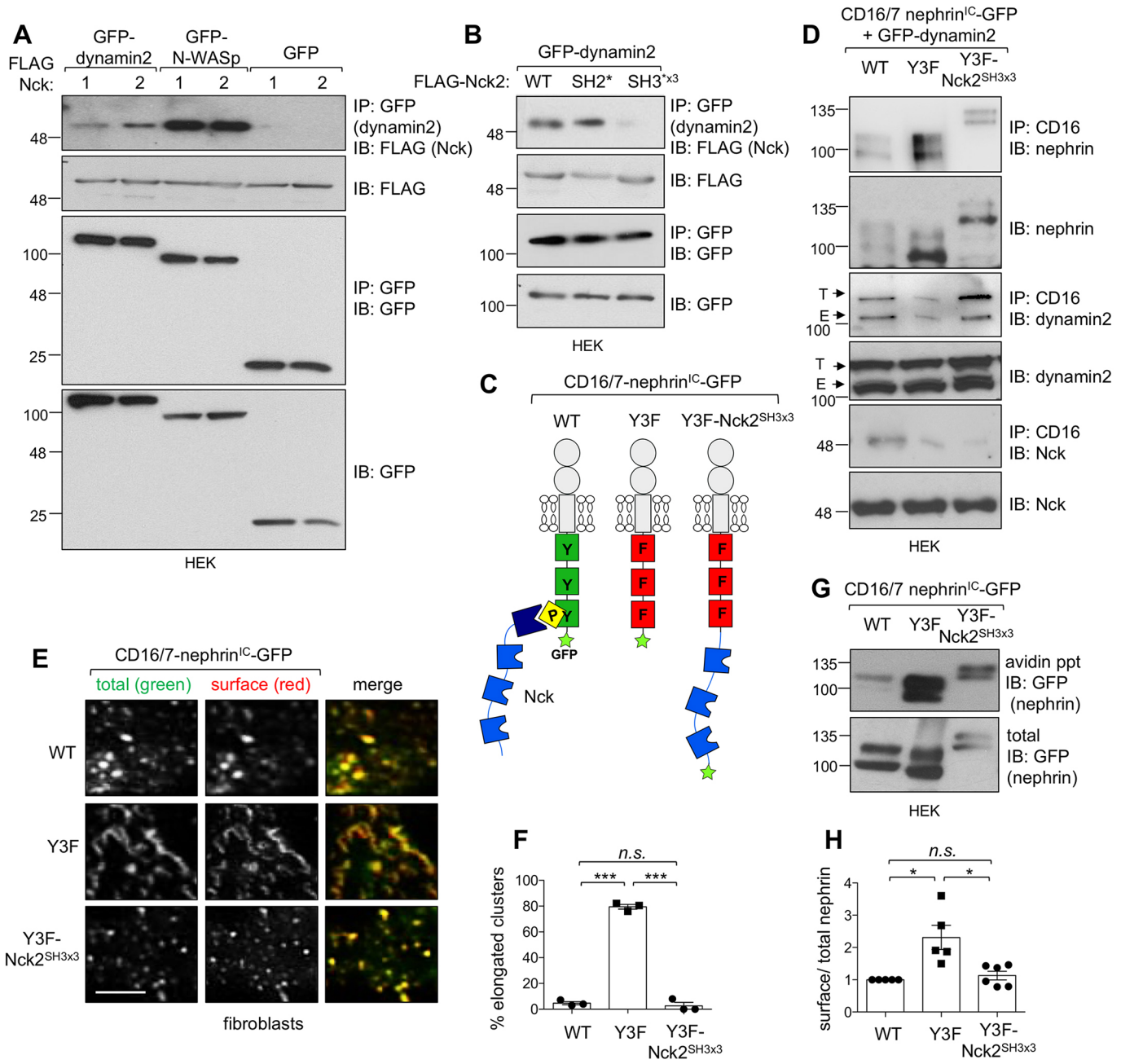

Fig. 6. Nck2 SH3 domains recruit dynamin-2, and can rescue the endocytosis defect induced by nephrin-Y3F mutation. (A) HEK293T cells were transfected with FLAG-tagged Nck1 or Nck2, along with GFP-tagged dynamin-2 or N-WASp, or GFP alone as a negative control. Lysates were immunoprecipitated (IP) for GFP, followed by IB as indicated. (B) HEK293T cells were transfected with FLAG-Nck2 variants and GFP-dynamin2 and processed as in A. Dynamin-2 binding is disrupted with the Nck2 SH3*x3 mutation. (C) Schematic showing signaling pathway wherein YDxV motifs on CD16-nephrin(WT)^{IC} recruit the SH2 domain of Nck (left), CD16-nephrin(Y3F)^{IC} unable to bind Nck (middle), and engineered fusion protein with Nck2 SH3 domains conjugated to CD16-nephrin(Y3F)^{IC} [referred to as CD16-nephrin(Y3F)^{IC}-Nck2(SH3x3)-GFP] (right). (D) HEK293T cells transfected with the constructs shown in C with GFP-dynamin2 to confirm interaction of endogenous ('E') and transfected ('T') dynamin-2 with the fusion protein and WT nephrin. (E) Total (green; post-permeabilization) and surface (red; pre-permeabilization) nephrin labeling of Nck1/2-null MEFs transfected with CD16/7-nephrin(WT)^{IC}-GFP, CD16/7-nephrin(Y3F)^{IC}-GFP or CD16-nephrin(Y3F)^{IC}-Nck2(SH3x3)-GFP, and stimulated with CD16 antibody. The fusion protein induces a punctate pattern comparable to WT, and unlike the poorly aggregated, elongated clusters seen with Y3F nephrin. Scale bar: 20 µm. (F) Quantification of the percentage of cells in E with elongated clusters (n=3 replicates/mutation). ***P<0.001 by one-way ANOVA with post-hoc Tukey's HSD test. n.s., not significant. (G) HEK293T cells transfected with the constructs shown in C were subjected to surface biotinylation, followed by lysis, streptavidin agarose precipitation (ppt) and immunoblotting (IB) as indicated. A portion of the initial lysate was saved to represent the total protein. (H) Densitometric quantification of surface/total nephrin from the data shown in G. Values are expressed relative to WT nephrin (n=5-6). *P<0.05 by Kruskal–Wallis test with post-hoc Dunn's Multiple Comparison test. n.s., not significant.

of dynamin-2 was reduced with nephrin-Y3F compared with nephrin-WT, and that the fusion protein could strongly associate with both transfected and endogenous dynamin in HEK cells (Fig. 6D). Next, CD16/7-nephrin(WT)^{IC}, CD16/7-nephrin(Y3F)^{IC} or CD16/7-nephrin(Y3F)^{IC}-Nck2(SH3x3) were independently expressed in Nck1/2-null MEFs, followed by CD16 cross-linking for 30 min and surface immunolabeling. Cells expressing the fusion protein showed nephrin clusters on the cell surface, which appeared

Journal of Cell Science

Journal of Cell Science (2020) 133, jcs236877. doi:10.1242/jcs.236877

similar albeit smaller than those with WT nephrin, and in sharp contrast to the elongated nephrin clusters induced by the Y3F mutant (Fig. 6E,F). Biotinylation experiments in HEK cells verify that surface nephrin levels are normalized by fusion of the Nck2 SH3 domains to nephrin-Y3F (Fig. 6G,H). In further support of this concept, addition of the TIR YDxV sequence, which recruits Nck to CD16/7-nephrin(Y3F)^{IC}, restored nephrin clusters to a punctate shape (Fig. S4), and we have shown previously that this protein/peptide fusion also restores actin polymerization (Blasutig et al., 2008). Together, these findings imply that nephrin-Nck interaction serves to localize SH3 effectors, including N-WASp and dynamin-2, which drive cluster formation and endocytosis.

Hyperphosphorylation of nephrin YDxV motifs *in vivo* triggers nephrin turnover and filtration barrier remodeling

Lastly, we set out to determine whether the interplay between nephrin phosphorylation and endocytosis seen in cultured cells might have physiological implications. To examine this, we employed a mouse model of reversible podocyte injury caused by injection of nephrotoxic serum (NTS), which correlates with transient permeability of the glomerular filtration barrier (proteinuria) and nephrin endocytosis (Haase et al., 2017; Königshausen et al., 2016). As we have reported previously (Keyvani Chahi et al., 2016), proteinuria peaked at 24 h post-NTS injection (Fig. 7A), although it could be detected as early as 6 h post-NTS injection (Fig. 7A). To characterize the kinetics of nephrin tyrosine phosphorylation and endocytosis at the onset of injury, mice were injected with NTS, and glomeruli were isolated from kidneys at 0 (baseline), 2, 4, 6 or 12 h post-injection for use in *ex vivo* biotinylation assays. Nephrin immunoblotting of avidin-precipitated samples demonstrates a significant loss of nephrin from the cell surface at 2 and 4 h post-injection, with a return to near baseline at 6 and 12 h post-injection (Fig. 7B,C). An inverse relationship was observed with nephrin phosphorylation on the Nck-binding sites, with an increase above baseline at 2 and 4 h post-injection, and a decrease at 6 and 12 h post-injection (Fig. 7B,D), which appeared to persist at 24 h post-injection, as reported previously (Keyvani Chahi et al., 2016). Given that dynamic changes in phosphorylation on the YDxV motifs appear to accompany filtration barrier remodeling, we reasoned that nephrin-Y3F mutant mice might show an altered response to NTS challenge. For these studies, we used young nephrin-Y3F animals, which do not show evidence of proteinuria (New et al., 2016). WT and nephrin-Y3F mice were injected with NTS or control IgG, and urine was collected at baseline or at 24 h post-injection. Remarkably, nephrin-Y3F mice did not develop significant NTS-induced proteinuria compared with WT counterparts (Fig. 7E,F), and they retained their foot process ultrastructure (Fig. 7G), unlike WT mice, which showed evidence of retraction. Altogether, these data demonstrate that hyperphosphorylation of nephrin YDxV motifs leads to rapid induction of nephrin endocytosis and subsequent remodeling of the filtration barrier.

DISCUSSION

In this article, we uncover a threshold effect of nephrin YDxV motifs and Nck SH3 domain signaling in controlling the assembly of membrane clusters and regulating endocytosis. We also show that dynamic changes in nephrin phosphorylation on the Nck-binding sites *in vivo* correlate with nephrin turnover in the slit diaphragm and filtration barrier remodeling. Taken together, our genetic and cell-based studies are the first to uncover a physiological function for this high valency signaling system.

The number of YDxV motifs on nephrin has been shown to correlate with phase separation in solution, wherein the presence of a tri- versus diphosphorylated nephrin tail lowers the concentrations of Nck and N-WASp required to reach the transition boundary for droplet formation (Banjade and Rosen, 2014; Li et al., 2012). Nephrin multivalency also appears to be necessary to increase the local density of Nck molecules within the phase-separated clusters, and in turn the stoichiometry-dependent dwell time and specific activity of associated effector proteins (Hilgemann et al., 2020; Oh et al., 2012; Rosendale et al., 2019). Our previous studies have demonstrated that a single nephrin YDxV motif is sufficient to bind Nck and induce actin polymerization (Blasutig et al., 2008); however, our present findings now indicate that phosphorylation of multiple motifs is required to drive endocytosis. We hypothesize that these distinct cellular outputs might reflect the dynamic composition of signaling effectors in nephrin clusters. Indeed, our data indicate that higher amounts of N-WASp than dynamin-2 are bound to Nck, suggesting that more nephrin/Nck clustering may be required to increase the dwell time and localized activity of dynamin-2. Furthermore, mutation of Y1217 alone, which is the YDxV motif most strongly associated with Nck (Jones et al., 2006), leads to a greater accumulation of irregular clusters than the Y1176 or Y1193 mutations. Lastly, the engineered CD16/7-nephrin(Y3F)^{IC}-Nck2(SH3x3)-GFP fusion protein shows smaller puncta than CD16/7-nephrin(WT)^{IC}, yet it is still able to bypass the clustering defect, likely because there is no dissociation between nephrin and Nck, and the dwell time of Nck-associated effector proteins is therefore increased. A similar rescue effect is seen with CD16/7-nephrin(Y3F)^{IC}-TIR-GFP, which inducibly binds Nck with notably higher affinity than nephrin YDxV sites (Blasutig et al., 2008). Intriguingly, recent studies support a link between phase separation and endocytosis, wherein droplet formation generates a force that drives invagination of the plasma membrane (Bergeron-Sandoval et al., 2018, preprint). We therefore suggest that threshold levels of nephrin/Nck clustering are required to facilitate endocytosis.

Our findings further indicate that multisite phosphorylation of nephrin modulates the potency of Nck signaling, as has been shown for the T-cell receptor and its signaling effectors (James, 2018; Su et al., 2016). Several previously identified feed-forward mechanisms may enhance the available valency within nephrin-Nck clusters. Notably, Nck expression can augment nephrin tyrosine phosphorylation, and this is dependent on Nck binding to nephrin via its SH2 domain while binding to Fyn kinase via its SH3 domains (New et al., 2013). In addition, Nck and N-WASp act cooperatively to relieve their respective intramolecular inhibitory conformations (Fig. 8). First, N-WASp relies on an Nck SH3 interdomain linker region for its ability to recruit and activate Arp2/3 (Okrut et al., 2015), and this linker also contributes to phase separation (Banjade et al., 2015). Next, the high-affinity binding of N-WASp to Nck disrupts the SH3-mediated autoinhibition of Nck (Takeuchi et al., 2010), which may in turn allow subsequent binding of low-affinity interactors, such as dynamin.

The association of nephrin phosphorylation and clustering with actin assembly has been established; however, their connection with endocytosis is less well understood (Swiatecka-Urban, 2017). Several studies have shown that nephrin phosphorylation regulates its trafficking (Espiritu et al., 2019; Martin et al., 2018; Qin et al., 2009; Quack et al., 2006), and that dynamin is required for both clathrin-dependent and raft-mediated nephrin endocytosis (Espiritu et al., 2019; Qin et al., 2009). Consistent with these findings, we show that Fyn induces removal of nephrin

Journal of Cell Science (2020) 133, jcs236877. doi:10.1242/jcs.236877

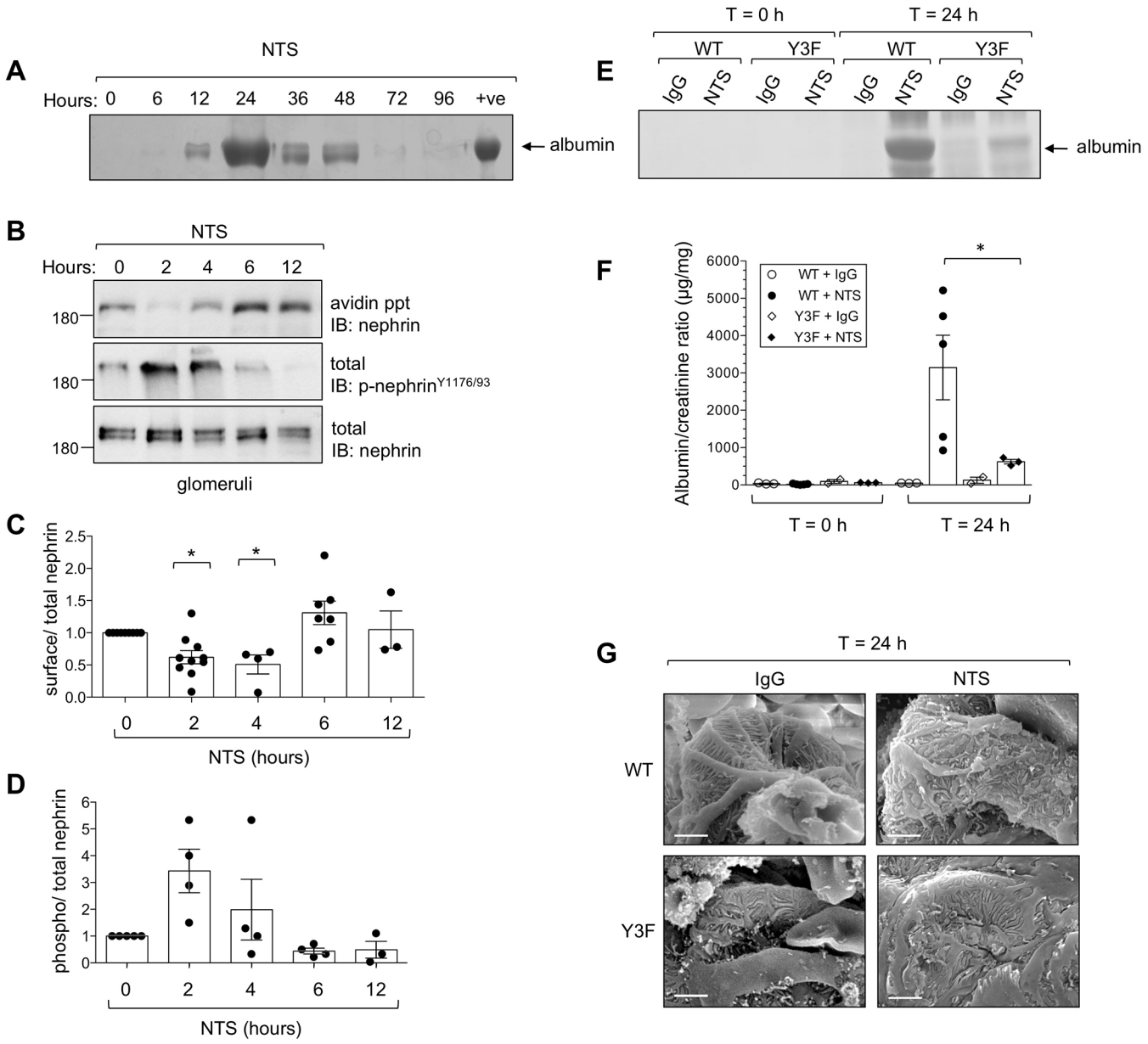

Fig. 7. Nephrin tyrosine phosphorylation correlates with endocytosis in a reversible kidney injury model. (A) Male mice were injected with nephrotoxic serum (NTS) and urine samples taken during the injury time course were resolved by SDS-PAGE followed by Coomassie Blue staining. Positive control is 2.5 µg of bovine serum albumin. (B) Glomeruli were isolated at 0 (n=4), 2 (n=10), 4 (n=4), 6 (n=6) and 12 (n=3) hours post-NTS injection, and subjected to surface biotinylation, followed by lysis, streptavidin agarose precipitation (ppt) and immunoblotting (IB) as indicated. A portion of the initial lysate was saved to represent the total protein. (C) Densitometric quantification of surface/total nephrin from the data shown in B. All values are expressed relative to surface nephrin levels at 0 h. *P<0.05, by Kruskal–Wallis test with post-hoc Dunn's multiple comparison test. (D) Densitometric quantification of phospho/total nephrin from the data shown in B (n=3-5/time point). All values are expressed relative to phospho-nephrin levels at 0 h. (E) Mice were injected with NTS or IgG control serum, and urine samples taken at 0 or 24 h post-injection were resolved by SDS-PAGE followed by Coomassie Blue staining. (F) Quantification of proteinuria using albumin/creatinine ratio (n=3-5/genotype). *P<0.05 by ANOVA. (G) Scanning electron micrographs of foot processes in WT and Y3F animals 24 h after injection with IgG or NTS. Scale bars: 2 µm.

from the cell surface, and that this effect is blocked with both the nephrin-Y3F mutant and the dynamin K44A mutant. Nephrin can be tethered by podocin into raft-like membrane clusters (Schwarz et al., 2001; Simons et al., 2001), and raft-mediated endocytosis has been proposed as a mechanism of slow internalization of phosphorylated nephrin following signal activation (Lahdenperä et al., 2003; Qin et al., 2009). By contrast, clathrin-mediated endocytosis is more rapid and may instead regulate steady-state recycling of nephrin (Espiritu et al., 2019; Satoh et al., 2014; Soda et al., 2012). We demonstrate that clathrin associates with nephrin clusters, and a recent study highlights a putative interaction between nephrin and clathrin (Espiritu et al., 2019). Altogether, our results support the cooperation of nephrin phosphorylation and endocytosis in slit diaphragm remodeling, and suggest that Nck functions at the interface of these signaling pathways.

Dynamin localization at actin tails requires its proline-rich region (Lee and De Camilli, 2002), and the arrested endocytic pits in dynamin-deficient MEFs are enriched for N-WASp, Arp2/3 and actin (Ferguson et al., 2009). In podocytes, Nck has been proposed

Journal of Cell Science (2020) 133, jcs236877. doi:10.1242/jcs.236877

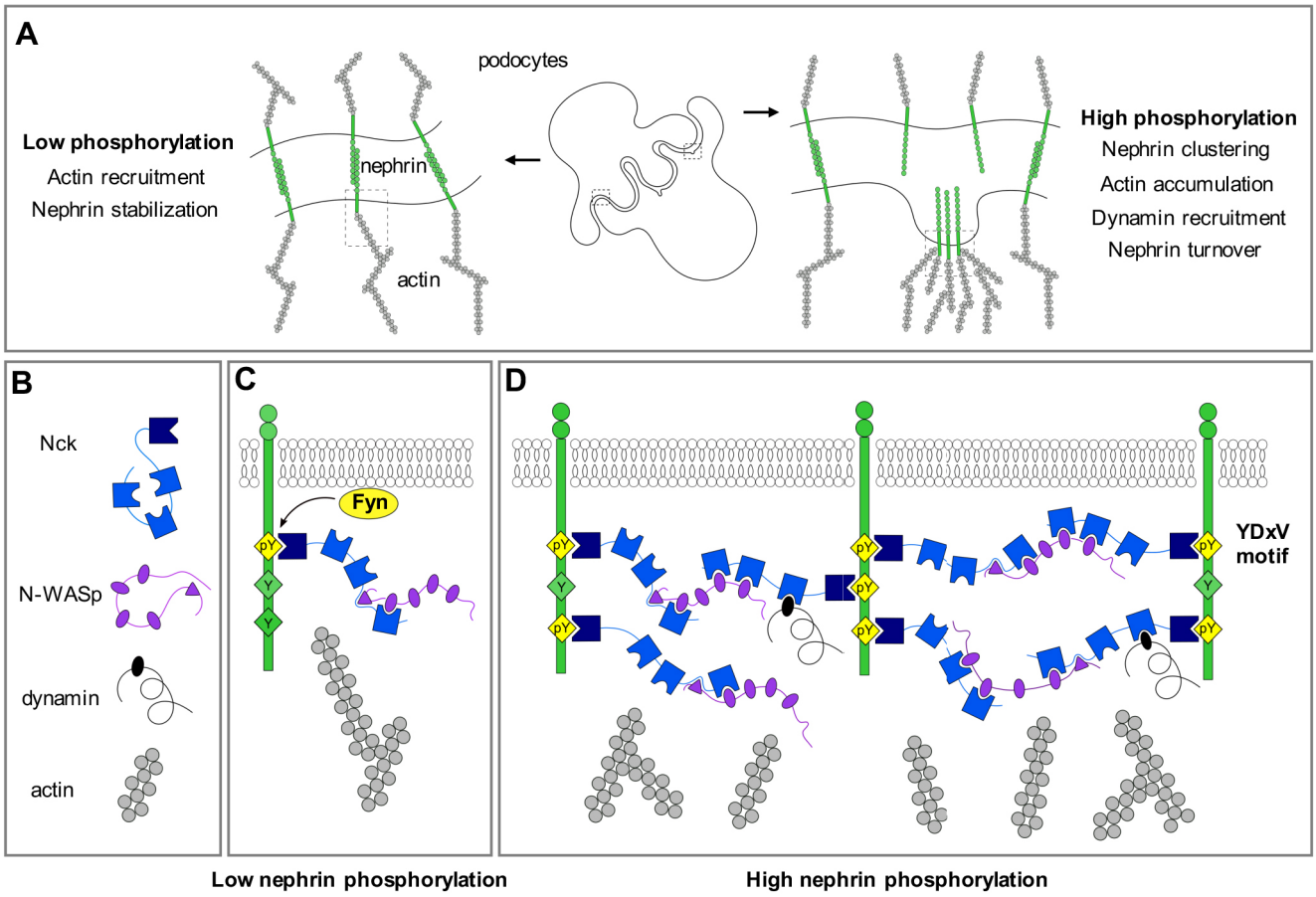

Fig. 8. Nephrin tyrosine multiplicity dictates differential roles for actin at the cell membrane. (A) Maintenance of the kidney's slit diaphragm (SD) barrier is dependent on a balance between stabilization and turnover of nephrin at the cell surface. Repetitive, *trans* nephrin-nephrin interactions, stabilized by the actin cytoskeleton, create pores in the SD, while nephrin clustering, driven by multivalent interactions, concentrates actin in nodes at the membrane and facilitates its endocytosis. (B) Nephrin's engagement with actin during these events is mediated via a network of kinase, adaptor and motor proteins, including Fyn, Nck, N-WASp and dynamin. Intramolecular inhibition of Nck and N-WASp regulates the recruitment of actin and endocytic machinery to nephrin, in part by limiting low-affinity interactions, such as between Nck and dynamin. (C) Recruitment of N-WASp to Nck releases these reciprocal inhibitions in a dose-dependent manner. When nephrin tyrosine phosphorylation is low, restricted recruitment of Nck and N-WASp facilitates a low level of actin polymerization that is sufficient to stabilize the SD. (D) Maximal nephrin tyrosine phosphorylation amplifies Nck/N-WASp interactions, which allows substantial actin accumulation along with dynamin recruitment. This contributes to membrane deformation during internalization of nephrin and, ultimately, vesicle scission.

as a linker protein between dynamin and nephrin at clathrin-coated pits (Soda et al., 2012), and an intermediary was similarly proposed to facilitate indirect interactions between tyrosine phosphorylated nephrin and dynamin in pancreatic β cells (Fornoni et al., 2010; Jeon et al., 2012). Our data suggest that the Nck SH3 domains couple dynamin to nephrin. Specifically, we demonstrate that expression of Nck SH3 domain mutants, which disrupt binding to N-WASp and dynamin-2, lead to defects in actin assembly and nephrin clustering, as we observed with nephrin-Y3F (Blasutig et al., 2008). As well, we show that direct fusion of the Nck SH3 domains or TIR YDxV sequence to nephrin-Y3F can restore dynamin-2 recruitment to nephrin and/or revert the clustering defects associated with mutant nephrin. It is tempting to speculate that the irregular clusters seen with the nephrin tyrosine mutants and Nck SH3 domain mutants, which have a tubular appearance, are continuous with the cell membrane, and colocalize with clathrin, in fact represent endocytic intermediates that fail to undergo dynamin-mediated fission.

Finally, our findings support the notion that a physiological relationship exists between the actin cytoskeleton and endocytosis in podocytes (Soda et al., 2012). Though the role of actin in endocytosis in mammalian cells is variable and thus debated (Aghamohammadzadeh and Ayscough, 2009; Dai and Sheetz, 1999), it is essential to counteract high membrane tension induced by stretch or at sites of strong adhesions, where actin filament assembly is proposed to provide the additional constriction force required to close the budding vesicle (Boulant et al., 2011). The lack of a uniform requirement for actin at endocytic sites may reflect multiple and possibly redundant mechanisms for the formation and fission of endosomes, as well as the local abundance of actin regulatory proteins, including N-WASp (Mooren et al., 2012). At sites where a dense meshwork of actin is present, such as focal adhesions, membrane deformation and movement may be restricted, and higher Arp2/3 activity (and possibly phase separation) may be required to generate and transmit sufficient force to pull the membrane inward (Mooren et al., 2012). This mechanism is likely of particular importance in the podocyte owing to the significant mechanical stretch and shear strain imposed on the slit diaphragm (Kriz and Lemley, 2017a,b), as well as the additional force needed to interrupt *trans* nephrin interactions (Endlich et al., 2017). Indeed, our findings in the NTS challenge model reveal a transient rise in nephrin phosphorylation on the YDxV motifs coincident with decreased nephrin surface expression and filtration barrier

remodeling. We hypothesize that this change in nephrin valency alters the composition and function of the slit diaphragm, to allow dynamic switching between nephrin stabilization and nephrin turnover (Fig. 8). Altogether, we posit that multivalent nephrin–Nck interactions serve to regulate the density of signaling effectors at the slit diaphragm to tune downstream signaling responses.

MATERIALS AND METHODS

Cell lines and culture conditions

Human embryonic kidney (HEK) 293T cells (from Tony Pawson, Lunenfeld-Tanenbaum Research Institute, Toronto) and Nck1/2 null MEFs (Jones et al., 2006) were grown in Dulbecco's high glucose modified eagle's medium (DMEM) supplemented with 10% fetal bovine serum (FBS) (both HyClone), 200 units/ml penicillin and 200 µg/ml streptomycin (Invitrogen) and maintained at 37°C with 5% CO_2. HEK cells were authenticated with GenePrint10 (Promega). Mouse podocyte cells (MPCs) were generated by isolating podocytes from Immortomouse [Charles River, official designation CBA;B10-Tg(H2Kb-tsA58)6Kio/Crl] according to standardized protocols (Shankland et al., 2007). MPCs were grown under permissive conditions in DMEF/12 (Hyclone) with 10% FBS, 200 units/ml penicillin, 200 µg/ml streptomycin (Invitrogen) and 20 units IFN-γ (Peprotech) at 33°C and 5% CO_2, then thermoswitched to 37°C with 2% FBS-containing medium for 10-14 days to induce differentiation. Cell lines were tested for the presence of *Mycoplasma*.

Transfections and transductions

Transient transfection of HEK293Ts was performed using polyethylenimine (PEI) for 24-48 h, whereas transfection of MEFs was performed using Lipofectamine 3000 (Invitrogen) as per manufacturer's specifications. Constructs encoding human FLAG-tagged NCK1 and NCK2, human Myc-tagged full-length and green fluorescent protein (GFP)-CD16/7-nephrin and fusions and mutants thereof were generated previously (Blasutig et al., 2008; Jones et al., 2006; Keyvani Chahi et al., 2016; Li et al., 2004). GFP-dynamin2-WT and GFP-dynamin2-K44A was provided by Dr Costin Antonescu (Ryerson University, Toronto, Canada) and GFP-N-WASp was provided by Dr Samantha Gruenheid (McGill University, Montreal, Canada). The AdEasy XL adenoviral system (Agilent Technologies) was utilized to generate all viruses in this study for transient expression in MPCs (Bi et al., 2014). Differentiated MPCs were infected with the indicated viruses at a dilution of 1:100 in 2% FBS-containing DMEF/12 over 15 h.

Cell stimulation and lysis

For CD16 clustering experiments, transfected or transduced cells were serum-starved (HEK293Ts or MEFs) or placed in 2% serum (MPCs) for 15 h before stimulation with 200 ng anti-CD16 antibody (Santa Cruz Biotechnology, sc-19620, clone 3G8) per ml medium containing 10% FBS for 30 min at 37°C. Cells were then placed on ice and lysed in cold PLC+ lysis buffer (PLC+) (50 mM HEPES pH 7.5, 150 mM NaCl, 10% glycerol, 1% Triton X-100, 15 mM $MgCl_2$, 1 mM EGTA, 10 mM NaPPi, 100 mM NaF) supplemented with fresh protease and phosphatase inhibitors (1 mM PMSF, 1 mM sodium orthovanadate, 10 µg/ml aprotinin and 10 µg/ml leupeptin) by sonicating on ice for 10 s, incubating on ice for 5 min, and centrifuging at 14,000 ***g*** for 10 min at 4°C. Protein concentrations in supernatants were determined using a bicinchoninic acid (BCA) Protein Assay (Pierce). Supernatants were mixed with appropriate amounts of SDS sample buffer and incubated at 100°C for 5 min.

Antibodies

Immunoprecipitation (IP) of GFP (Abcam, 290) was performed using protein A beads for 1 h at 4°C with rotation. IP of CD16 (Santa Cruz Biotechnology, sc-19620, clone 3G8) was performed using mouse beads overnight at 4°C with rotation. IP incubations were followed by washing three times with PLC+ and protein complexes were eluted from the beads in 2× SDS loading buffer by boiling at 100°C for 2 min prior to proceeding to immunoblotting (IB). For IB, PVDF membranes were incubated with the following primary antibodies overnight at 4°C: goat anti-dynamin2 (Santa Cruz Biotechnology, sc-6400, 1:1000); rabbit anti-nephrin (a gift from Dr Tomoko Takano, McGill University, Montreal, Canada; 1:1000), rabbit anti-Nck (a gift from Dr Louise Larose, McGill University, Montreal, Canada; 1:1000) or anti-pY1176/1193 (Abcam, ab80299, 1:1000), mouse anti-FLAG M2 (Sigma-Aldrich, F3165, 1:2000), anti-myc 9E10 (Millipore, 05-419, 1:1000), anti-GFP B2 (Santa Cruz Biotechnology, sc-9996, 1:1000) or anti-pY 4G10 (Upstate Biotechnology, 16-101, 1:1000). After washing, secondary horseradish peroxidase (HRP)-conjugated donkey anti-goat (sc-2020, Santa Cruz Biotechnology), goat anti-rabbit (170-6515, Bio-Rad) or goat anti-mouse (170-6516, Bio-Rad), antibodies were used at 1:10,000 in TBST for 1 h at room temperature. Signals were detected using ECL (Pierce) and imaged using a ChemiDoc XRS+ (Bio-Rad) or exposed to film (Pierce). Densitometry was performed using ImageLab version 2.0 analysis software (Bio-Rad).

Nephrin-Y3F animals

Nephrin-Y3F knock-in mice were generated by homologous recombination targeting mutation of mouse Y1191, Y1208 and Y1232 (corresponding to human Y1176, Y1193 and Y1217) to phenylalanine (F) as described previously (New et al., 2016) and back-crossed onto the CD-1 (official designation CD-1.B6;129Nphs1,Tm1.1./Njns) or C57BL/6N backgrounds. Both male and female animals were used unless otherwise noted. No statistical method was used to predetermine the sample size. The investigators were not blinded to animal genotypes or assignments, and no animals were excluded from the study. All animal studies were carried out in accordance with Canadian Council on Animal Care protocols and approved by the University of Guelph Animal Care Committee (Animal Use Protocol 3291).

Nephrotoxic serum nephrosis

Non-proteinuric male WT or nephrin-Y3F mice (both C57BL/6N) aged 8-10 weeks were injected with 0.04 mg/g of IgG γ2 subclass sheep anti-rat nephrotoxic serum (a gift from Dr David Salant, Boston University School of Medicine, MA, USA) or an equivalent dose of normal sheep IgG serum as a control (Capralogics, SG0010) via tail vein injection. Spot urine samples were collected prior to and at several time points after injection. Mice were euthanized with CO_2 at the indicated time points and kidneys were removed and immediately processed for analysis.

Evaluation of proteinuria

Mice were placed into a metabolic cage until they urinated freely, and spot urines were collected. For Coomassie urine gels, urine samples (2 or 5 µl) were diluted in sodium dodecyl sulfate (SDS) sample buffer, separated by 10% SDS-polyacrylamide gel electrophoresis (PAGE), and stained with Coomassie Brilliant Blue R. The urinary albumin/creatinine ratio was determined using the Albuwell M enzyme-linked immunosorbent assay (ELISA) (Exocell) and Creatinine Companion (Exocell) kits according to the manufacturer's instructions.

Biotinylation experiments

Isolated glomeruli or adherent cells were subjected to biotinylation and avidin precipitation as described previously (Martin et al., 2018). Where indicated, cells were stimulated with CD16 antibody at 37°C for 30 min unless otherwise noted as described in 'Cell stimulation and lysis' above. Subsequently, cell-surface proteins were biotinylated at 4°C for 45 min before lysis and avidin precipitation as described previously (Martin et al., 2018). Quantification of surface nephrin in each sample was determined by dividing the density of band observed in immunoblotting of the streptavidin-precipitated sample by the density of band observed in the input sample. The ratio of this value in test samples to the value obtained in control samples was calculated and represents the amount of surface nephrin in the indicated test groups relative to control samples.

Microscopy

Where indicated, cells were stimulated with CD16 antibody at 37°C for 30 min unless otherwise noted as described in 'Cell stimulation and lysis' above. For indirect immunofluorescence experiments, cells were first gently washed three times in PBS to remove residual CD16 antibody prior to further processing. Slides were then fixed for 10 min in 4%

paraformaldehyde before being permeabilized in 1% Triton X-100 for 10 min to stain surface and cytosolic proteins or left unpermeabilized to label surface proteins. Samples were then blocked for 1 h in 10% goat serum, incubated with the indicated primary antibody and/or Texas Red phalloidin for 1 h followed by appropriate secondary antibodies (1:400) for 1 h and finally mounted using Prolong Gold mounting medium (Invitrogen), with intermediary washes in PBS. To view surface nephrin, cells transfected with various GFP-CD16/7-nephrin constructs (visible in the 488 wavelength) were stimulated with mouse anti-CD16 antibody at 37°C for 30 min, then cold-stained with anti-mouse Alexa Fluor 594 (to label surface nephrin in the 594 wavelength) prior to fixation and mounting. Where applicable, cells were also stained with rabbit anti-clathrin (Cell Signaling, 4796) and anti-rabbit Alex Fluor 647. In the merged immunofluorescent image, surface nephrin, which appears in both the 488 (total, green) and 594 (surface alone, red) channels, appears yellow, whereas endogenous nephrin, protected from anti-mouse Alexa Fluor 594 labeling, remains green. Epifluoresence images were obtained using Volocity software version 5.3.2 (Improvision) on a DMIRE2 microscope (Leica) using a 40× objective. Stacks were captured at 0.2 µm *z*-intervals, then deconvoluted using iterative restoration (95% confidence with 15 iterations) in Volocity. Confocal images were obtained using the 60× objective (oil immersion) with EZ-C1 software on a Nikon Eclipse Ti microscope.

For quantification of cluster morphology, cells containing non-spherical or irregular-shaped clusters were scored as positive for elongated clusters. The percentage of total cells scored as positive for elongated clusters was determined for each condition. A minimum of 100 cells per replicate were scored for MEFs and 50 cells per replicate for podocytes.

For SR-SIM imaging, kidneys were fixed in 4% paraformaldehyde and embedded in paraffin prior to sectioning. Prior to staining, slides were blocked for 1 h in 10% goat serum, then incubated with respective antibodies for 1 h. After three washes in PBS, slides were incubated with anti-rabbit secondary antibodies (1:400) for 1 h. Slides were washed, then mounted using Prolong Gold anti-fade mounting medium (Invitrogen). SR-SIM images were obtained using an Elyra LSM 880 microscope (Zeiss) and processed with ZEN software (Zeiss) to obtain the SIM.

For electron microscopy (EM), kidney tissue was fixed in 0.1 M sodium cacodylate buffer containing 4% paraformaldehyde and 2% glutaraldehyde (Electron Microscopy Sciences), post-fixed in 1% OsO_4, and dehydrated through graded ethanols. Transmission EM samples were embedded in Quetol–Spurr resin. Ultrathin sections were cut and stained with uranyl acetate and lead citrate and viewed using an FEI CM100 TEM. For scanning EM, samples were critical point dried and sputter coated with gold. Samples were viewed using a Hitachi S-540 SEM.

Statistical analyses

Data are reported as arithmetic mean±s.e.m. Data analysis was performed using GraphPad Prism version 5 and SAS version 9.4. For all analyses, $P<0.05$ was considered statistically significant. Two groups were compared using unpaired Student's *t*-test when data followed a Gaussian distribution; when it did not, data were analyzed using Mann–Whitney test where variances differed. When data were normalized so that all control values were identical, the one-sample *t*-test was used. Three or more groups were analyzed using ANOVA (analysis of variance) with post-hoc Tukey's HSD test when data followed a Gaussian distribution; where it did not, or when values were normalized to the control, data were analyzed using the non-parametric ANOVA Kruskal–Wallis test with post-hoc Dunn's Multiple Comparison test (Curtis et al., 2018).

Acknowledgements

We gratefully acknowledge C. Antonescu, S. Gruenheid, L. Larose and D. Salant for providing reagents; M. Krendel for training in viral construction; P. Lu for technical support; and J. McGlade for critical review of the manuscript.

Competing interests

The authors declare no competing or financial interests.

Author contributions

Conceptualization: C.E.M., L.A.N., N.J.; Methodology: C.E.M., L.A.N., N.J.; Formal analysis: C.E.M., L.A.N., N.J.P., A.K.C., A.E.M., T.T., I.M.B., N.J.; Investigation: C.E.M., L.A.N., N.J.P., A.K.C., A.E.M., T.T., I.M.B., N.J.; Resources: T.P., N.J.; Data curation: C.E.M., L.A.N.; Writing - original draft: C.E.M., L.A.N., N.J.; Writing - review & editing: C.E.M., L.A.N., A.K.C., N.J.; Supervision: T.P., N.J.; Project administration: N.J.; Funding acquisition: N.J.

Funding

This work was supported by grants from the Canadian Institutes of Health Research (PJT-148731 to N.J.) and the Kidney Foundation of Canada (KFOC-110007 to N.J., KFOC-180016 to T.T.). N.J. holds a Tier 2 Canada Research Chair in Eukaryotic Cellular Signaling and was the recipient of a CIHR/KRESCENT New Investigator Award. CEM and LAN were supported by NSERC Alexander Graham Bell Canada Graduate Doctoral Scholarships.

Supplementary information

Supplementary information available online at
http://jcs.biologists.org/lookup/doi/10.1242/jcs.236877.supplemental

References

Aghamohammadzadeh, S. and Ayscough, K. R. (2009). Differential requirements for actin during yeast and mammalian endocytosis. *Nat. Cell Biol.* **11**, 1039-1042. doi:10.1038/ncb1918

Banjade, S. and Rosen, M. K. (2014). Phase transitions of multivalent proteins can promote clustering of membrane receptors. *eLife* **3**, e04123. doi:10.7554/eLife.04123

Banjade, S., Wu, Q., Mittal, A., Peeples, W. B., Pappu, R. V. and Rosen, M. K. (2015). Conserved interdomain linker promotes phase separation of the multivalent adaptor protein Nck. *Proc. Natl. Acad. Sci. USA* **112**, E6426-E6435. doi:10.1073/pnas.1508778112

Bergeron-Sandoval, L.-P., Khadivi Heris, H., Chang, C., Cornell, C. E., Keller, S. L., François, P., Hendricks, A. G., Ehrlicher, A. J., Pappu, R. V. and Michnick, S. W. (2018). Endocytosis caused by liquid-liquid phase separation of proteins. *BioRxiv*. doi:10.1101/145664

Bi, J., Pellenz, C. D. and Krendel, M. (2014). Visualization of cytoskeletal dynamics in podocytes using adenoviral vectors. *Cytoskeleton* **71**, 145-156. doi:10.1002/cm.21162

Blasutig, I. M., New, L. A., Thanabalasuriar, A., Dayarathna, T. K., Goudreault, M., Quaggin, S. E., Li, S. S.-C., Gruenheid, S., Jones, N. and Pawson, T. (2008). Phosphorylated YDXV motifs and Nck SH2/SH3 adaptors act cooperatively to induce actin reorganization. *Mol. Cell. Biol.* **28**, 2035-2046. doi:10.1128/MCB.01770-07

Boulant, S., Kural, C., Zeeh, J.-C., Ubelmann, F. and Kirchhausen, T. (2011). Actin dynamics counteract membrane tension during clathrin-mediated endocytosis. *Nat. Cell Biol.* **13**, 1124-1131. doi:10.1038/ncb2307

Case, L. B., Zhang, X., Ditlev, J. A. and Rosen, M. K. (2019). Stoichiometry controls activity of phase-separated clusters of actin signaling proteins. *Science* **363**, 1093-1097. doi:10.1126/science.aau6313

Curtis, M. J., Alexander, S., Cirino, G., Docherty, J. R., George, C. H., Giembycz, M. A., Hoyer, D., Insel, P. A., Izzo, A. A., Ji, Y. et al. (2018). Experimental design and analysis and their reporting II: updated and simplified guidance for authors and peer reviewers. *Br. J. Pharmacol.* **175**, 987-993. doi:10.1111/bph.14153

Dai, J. and Sheetz, M. P. (1999). Membrane tether formation from blebbing cells. *Biophys. J.* **77**, 3363-3370. doi:10.1016/S0006-3495(99)77168-7

Ditlev, J. A., Michalski, P. J., Huber, G., Rivera, G. M., Mohler, W. A., Loew, L. M. and Mayer, B. J. (2012). Stoichiometry of Nck-dependent actin polymerization in living cells. *J. Cell Biol.* **197**, 643-658. doi:10.1083/jcb.201111113

Endlich, K., Kliewe, F. and Endlich, N. (2017). Stressed podocytes – mechanical forces, sensors, signaling and response. *Pflugers Arch.* **469**, 937-949. doi:10.1007/s00424-017-2025-8

Espiritu, E. B., Jiang, H., Moreau-Marquis, S., Sullivan, M., Yan, K., Beer Stolz, D., Sampson, M. G., Hukriede, N. A. and Swiatecka-Urban, A. (2019). The human nephrin Y1139RSL motif is essential for podocyte foot process organization and slit diaphragm formation during glomerular development. *J. Biol. Chem.* **294**, 10773-10788. doi:10.1074/jbc.RA119.008235

Ferguson, S. M. and De Camilli, P. (2012). Dynamin, a membrane-remodelling GTPase. *Nat. Rev. Mol. Cell Biol.* **13**, 75-88. doi:10.1038/nrm3266

Ferguson, S. M., Ferguson, S., Raimondi, A., Paradise, S., Shen, H., Mesaki, K., Ferguson, A., Destaing, O., Ko, G., Takasaki, J. et al. (2009). Coordinated actions of actin and BAR proteins upstream of dynamin at endocytic clathrin-coated pits. *Dev. Cell* **17**, 811-822. doi:10.1016/j.devcel.2009.11.005

Fornoni, A., Jeon, J., Varona Santos, J., Cobianchi, L., Jauregui, A., Inverardi, L., Mandic, S. A., Bark, C., Johnson, K., McNamara, G. et al. (2010). Nephrin is expressed on the surface of insulin vesicles and facilitates glucose-stimulated insulin release. *Diabetes* **59**, 190-199. doi:10.2337/db09-0655

Haase, R., Potthoff, S. A., Meyer-Schwesinger, C., Frosch, C., Wiech, T., Panzer, U., Königshausen, E., Stegbauer, J., Sellin, L., Rump, L. C. et al. (2017). A novel in vivo method to quantify slit diaphragm protein abundance in murine proteinuric kidney disease. *PLoS ONE* **12**, e0179217. doi:10.1371/journal.pone.0179217

Hilgemann, D. W., Lin, M.-J., Fine, M. and Deisl, C. (2020). On the existence of endocytosis driven by membrane phase separations. *Biochim. Biophys. Acta Biomembr.* **1862**, 183007. doi:10.1016/j.bbamem.2019.06.006
James, J. R. (2018). Tuning ITAM multiplicity on T cell receptors can control potency and selectivity to ligand density. *Sci. Signal.* **11**, eaan1088. doi:10.1126/scisignal.aan1088
Jeon, J., Leibiger, I., Moede, T., Walter, B., Faul, C., Maiguel, D., Villarreal, R., Guzman, J., Berggren, P.-O., Mundel, P. et al. (2012). Dynamin-mediated Nephrin phosphorylation regulates glucose-stimulated insulin release in pancreatic beta cells. *J. Biol. Chem.* **287**, 28932-28942. doi:10.1074/jbc.M112.389452
Jones, N., Blasutig, I. M., Eremina, V., Ruston, J. M., Bladt, F., Li, H., Huang, H., Larose, L., Li, S. S.-C., Takano, T. et al. (2006). Nck adaptor proteins link nephrin to the actin cytoskeleton of kidney podocytes. *Nature* **440**, 818-823. doi:10.1038/nature04662
Jones, N., New, L. A., Fortino, M. A., Eremina, V., Ruston, J., Blasutig, I. M., Aoudjit, L., Zou, Y., Liu, X., Yu, G.-L. et al. (2009). Nck proteins maintain the adult glomerular filtration barrier. *J. Am. Soc. Nephrol.* **20**, 1533-1543. doi:10.1681/ASN.2009010056
Keyvani Chahi, A., Martin, C. E. and Jones, N. (2016). Nephrin suppresses Hippo signaling through the adaptor proteins Nck and WTIP. *J. Biol. Chem.* **291**, 12799-12808. doi:10.1074/jbc.M116.724245
Königshausen, E., Zierhut, U. M., Ruetze, M., Potthoff, S. A., Stegbauer, J., Woznowski, M., Quack, I., Rump, L. C. and Sellin, L. (2016). Angiotensin II increases glomerular permeability by β-arrestin mediated nephrin endocytosis. *Sci. Rep.* **6**, 39513. doi:10.1038/srep39513
Kriz, W. and Lemley, K. V. (2017a). Mechanical challenges to the glomerular filtration barrier: adaptations and pathway to sclerosis. *Pediatr. Nephrol.* **32**, 405-417. doi:10.1007/s00467-016-3358-9
Kriz, W. and Lemley, K. V. (2017b). Potential relevance of shear stress for slit diaphragm and podocyte function. *Kidney Int.* **91**, 1283-1286. doi:10.1016/j.kint.2017.02.032
Lahdenperä, J., Kilpeläinen, P., Liu, X. L., Pikkarainen, T., Reponen, P., Ruotsalainen, V. and Tryggvason, K. (2003). Clustering-induced tyrosine phosphorylation of nephrin by Src family kinases. *Kidney Int.* **64**, 404-413. doi:10.1046/j.1523-1755.2003.00097.x
Lee, E. and De Camilli, P. (2002). Dynamin at actin tails. *Proc. Natl. Acad. Sci. USA* **99**, 161-166. doi:10.1073/pnas.012607799
Li, H., Lemay, S., Aoudjit, L., Kawachi, H. and Takano, T. (2004). SRC-family kinase Fyn phosphorylates the cytoplasmic domain of nephrin and modulates its interaction with podocin. *J. Am. Soc. Nephrol.* **15**, 3006-3015. doi:10.1097/01.ASN.0000146689.88078.80
Li, P., Banjade, S., Cheng, H.-C., Kim, S., Chen, B., Guo, L., Llaguno, M., Hollingsworth, J. V., King, D. S., Banani, S. F. et al. (2012). Phase transitions in the assembly of multivalent signalling proteins. *Nature* **483**, 336-340. doi:10.1038/nature10879
Martin, C. E., Petersen, K. A., Aoudjit, L., Tilak, M., Eremina, V., Hardy, W. R., Quaggin, S. E., Takano, T. and Jones, N. (2018). ShcA adaptor protein promotes nephrin endocytosis and is upregulated in proteinuric nephropathies. *J. Am. Soc. Nephrol.* **29**, 92-103. doi:10.1681/ASN.2017030285
Mayer, B. J. and Yu, J. (2018). Protein clusters in phosphotyrosine signal transduction. *J. Mol. Biol.* **430**, 4547-4556. doi:10.1016/j.jmb.2018.05.040
Mooren, O. L., Galletta, B. J. and Cooper, J. A. (2012). Roles for actin assembly in endocytosis. *Annu. Rev. Biochem.* **81**, 661-686. doi:10.1146/annurev-biochem-060910-094416
New, L. A., Keyvani Chahi, A. and Jones, N. (2013). Direct regulation of nephrin tyrosine phosphorylation by Nck adaptor proteins. *J. Biol. Chem.* **288**, 1500-1510. doi:10.1074/jbc.M112.439463
New, L. A., Martin, C. E. and Jones, N. (2014). Advances in slit diaphragm signaling. *Curr. Opin. Nephrol. Hypertens.* **23**, 420-430. doi:10.1097/01.mnh.0000447018.28852.b6
New, L. A., Martin, C. E., Scott, R. P., Platt, M. J., Keyvani Chahi, A., Stringer, C. D., Lu, P., Samborska, B., Eremina, V., Takano, T. et al. (2016). Nephrin tyrosine phosphorylation is required to stabilize and restore podocyte foot process architecture. *J. Am. Soc. Nephrol.* **27**, 2422-2435. doi:10.1681/ASN.2015091048
Nishibori, Y., Liu, L. I., Hosoyamada, M., Endou, H., Kudo, A., Takenaka, H., Higashihara, E., Bessho, F., Takahashi, S., Kershaw, D. et al. (2004). Disease-causing missense mutations in NPHS2 gene alter normal nephrin trafficking to the plasma membrane. *Kidney Int.* **66**, 1755-1765. doi:10.1111/j.1523-1755.2004.00898.x
Oh, D., Ogiue-Ikeda, M., Jadwin, J. A., Machida, K., Mayer, B. J. and Yu, J. (2012). Fast rebinding increases dwell time of Src homology 2 (SH2)-containing proteins near the plasma membrane. *Proc. Natl. Acad. Sci. USA* **109**, 14024-14029. doi:10.1073/pnas.1203397109
Ohashi, T., Uchida, K., Asamiya, Y., Tsuruta, Y., Ohno, M., Horita, S. and Nitta, K. (2010). Phosphorylation status of nephrin in human membranous nephropathy. *Clin. Exp. Nephrol.* **14**, 51-55. doi:10.1007/s10157-009-0241-z
Okrut, J., Prakash, S., Wu, Q., Kelly, M. J. S. and Taunton, J. (2015). Allosteric N-WASp activation by an inter-SH3 domain linker in Nck. *Proc. Natl. Acad. Sci. USA* **112**, E6436-E6445. doi:10.1073/pnas.1510876112
Qin, X.-S., Tsukaguchi, H., Shono, A., Yamamoto, A., Kurihara, H. and Doi, T. (2009). Phosphorylation of nephrin triggers its internalization by raft-mediated endocytosis. *J. Am. Soc. Nephrol.* **20**, 2534-2545. doi:10.1681/ASN.2009010011
Quack, I., Rump, L. C., Gerke, P., Walther, I., Vinke, T., Vonend, O., Grunwald, T. and Sellin, L. (2006). beta-Arrestin2 mediates nephrin endocytosis and impairs slit diaphragm integrity. *Proc. Natl. Acad. Sci. USA* **103**, 14110-14115. doi:10.1073/pnas.0602587103
Rohatgi, R., Nollau, P., Ho, H.-Y. H., Kirschner, M. W. and Mayer, B. J. (2001). Nck and phosphatidylinositol 4,5-bisphosphate synergistically activate actin polymerization through the N-WASp-Arp2/3 pathway. *J. Biol. Chem.* **276**, 26448-26452. doi:10.1074/jbc.M103856200
Rosendale, M., Van, T. N. N., Grillo-Bosch, D., Sposini, S., Claverie, L., Gauthereau, I., Claverol, S., Choquet, D., Sainlos, M. and Perrais, D. (2019). Functional recruitment of dynamin requires multimeric interactions for efficient endocytosis. *Nat. Commun.* **10**, 4462. doi:10.1038/s41467-019-12434-9
Satoh, D., Hirose, T., Harita, Y., Daimon, C., Harada, T., Kurihara, H., Yamashita, A. and Ohno, S. (2014). aPKCλ maintains the integrity of the glomerular slit diaphragm through trafficking of nephrin to the cell surface. *J. Biochem.* **156**, 115-128. doi:10.1093/jb/mvu022
Schell, C., Baumhakl, L., Salou, S., Conzelmann, A.-C., Meyer, C., Helmstädter, M., Wrede, C., Grahammer, F., Eimer, S., Kerjaschki, D. et al. (2013). N-wasp is required for stabilization of podocyte foot processes. *J. Am. Soc. Nephrol.* **24**, 713-721. doi:10.1681/ASN.2012080844
Schwarz, K., Simons, M., Reiser, J., Saleem, M. A., Faul, C., Kriz, W., Shaw, A. S., Holzman, L. B. and Mundel, P. (2001). Podocin, a raft-associated component of the glomerular slit diaphragm, interacts with CD2AP and nephrin. *J. Clin. Invest.* **108**, 1621-1629. doi:10.1172/JCI200112849
Scott, R. P. and Quaggin, S. E. (2015). Review series: the cell biology of renal filtration. *J. Cell Biol.* **209**, 199-210. doi:10.1083/jcb.201410017
Shankland, S. J., Pippin, J. W., Reiser, J. and Mundel, P. (2007). Podocytes in culture: past, present, and future. *Kidney Int.* **72**, 26-36. doi:10.1038/sj.ki.5002291
Shimizu, J., Tanaka, H., Aya, K., Ito, S., Sado, Y. and Seino, Y. (2002). A missense mutation in the nephrin gene impairs membrane targeting. *Am. J. Kidney Dis.* **40**, 697-703. doi:10.1053/ajkd.2002.35676
Simons, M., Schwarz, K., Kriz, W., Miettinen, A., Reiser, J., Mundel, P. and Holthöfer, H. (2001). Involvement of lipid rafts in nephrin phosphorylation and organization of the glomerular slit diaphragm. *Am. J. Pathol.* **159**, 1069-1077. doi:10.1016/S0002-9440(10)61782-8
Soda, K. and Ishibe, S. (2013). The function of endocytosis in podocytes. *Curr. Opin. Nephrol. Hypertens.* **22**, 432-438. doi:10.1097/MNH.0b013e3283624820
Soda, K., Balkin, D. M., Ferguson, S. M., Paradise, S., Milosevic, I., Giovedi, S., Volpicelli-Daley, L., Tian, X., Wu, Y., Ma, H. et al. (2012). Role of dynamin, synaptojanin, and endophilin in podocyte foot processes. *J. Clin. Invest.* **122**, 4401-4411. doi:10.1172/JCI65289
Su, X., Ditlev, J. A., Hui, E., Xing, W., Banjade, S., Okrut, J., King, D. S., Taunton, J., Rosen, M. K. and Vale, R. D. (2016). Phase separation of signaling molecules promotes T cell receptor signal transduction. *Science* **352**, 595-599. doi:10.1126/science.aad9964
Svitkina, T. M. and Borisy, G. G. (1999). Arp2/3 complex and actin depolymerizing factor/cofilin in dendritic organization and treadmilling of actin filament array in lamellipodia. *J. Cell Biol.* **145**, 1009-1026. doi:10.1083/jcb.145.5.1009
Swiatecka-Urban, A. (2017). Endocytic trafficking at the mature podocyte slit diaphragm. *Front. Pediatr.* **5**, 32. doi:10.3389/fped.2017.00032
Takeuchi, K., Sun, Z.-Y. J., Park, S. and Wagner, G. (2010). Autoinhibitory interaction in the multidomain adaptor protein Nck: possible roles in improving specificity and functional diversity. *Biochemistry* **49**, 5634-5641. doi:10.1021/bi100322m
Uchida, K., Suzuki, K., Iwamoto, M., Kawachi, H., Ohno, M., Horita, S. and Nitta, K. (2008). Decreased tyrosine phosphorylation of nephrin in rat and human nephrosis. *Kidney Int.* **73**, 926-932. doi:10.1038/ki.2008.19
Verma, R., Wharram, B., Kovari, I., Kunkel, R., Nihalani, D., Wary, K. K., Wiggins, R. C., Killen, P. and Holzman, L. B. (2003). Fyn binds to and phosphorylates the kidney slit diaphragm component Nephrin. *J. Biol. Chem.* **278**, 20716-20723. doi:10.1074/jbc.M301689200
Wernerson, A., Dunér, F., Pettersson, E., Widholm, S. M., Berg, U., Ruotsalainen, V., Tryggvason, K., Hultenby, K. and Söderberg, M. (2003). Altered ultrastructural distribution of nephrin in minimal change nephrotic syndrome. *Nephrol. Dial. Transplant.* **18**, 70-76. doi:10.1093/ndt/18.1.70
Wunderlich, L., Faragó, A. and Buday, L. (1999). Characterization of interactions of Nck with Sos and dynamin. *Cell. Signal.* **11**, 25-29. doi:10.1016/S0898-6568(98)00027-8

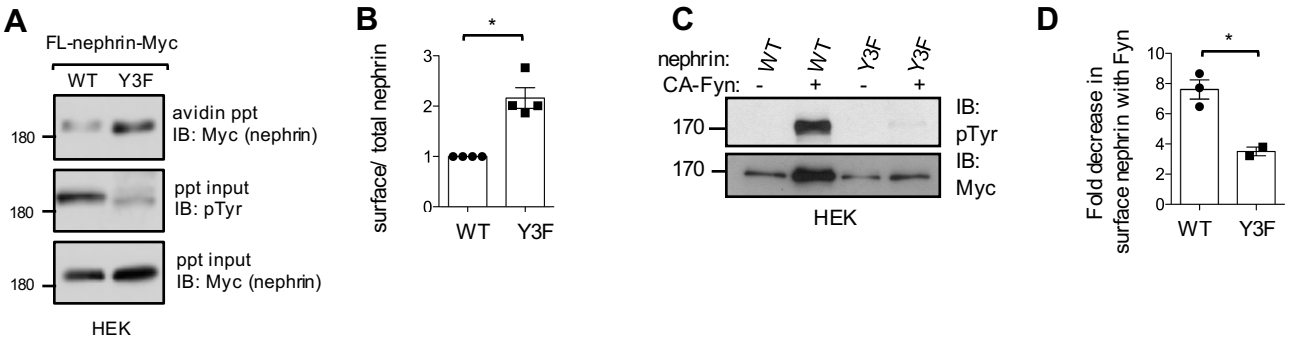

Figure S1. (A) Transfected HEK 293Ts with full-length nephrin constructs were subjected to surface biotinylation, followed by lysis, streptavidin agarose precipitation (ppt) and immunoblotting (IB) as indicated. A portion of the initial lysate was saved to represent the input / total lysate. (B) Densitometric quantitation of surface/ total nephrin from (A). Y3F values were made relative to WT (n=4). *P<0.05 by one-sample *t*-test (C,D) Nephrin phosphorylation results in increased nephrin endocytosis. (C) HEK cells were transfected with the indicated full-length nephrin and Fyn constructs. Western blot showing Fyn-mediated increase in nephrin tyrosine phosphorylation. Samples were also subjected to surface biotinylation as in A. (D) Densitometric quantitation of fold change in surface nephrin internalization with Fyn from (C). Nephrin-Y3F (n=2) has a decreased rate of Fyn-mediated nephrin internalization compared to nephrin-WT (n=3). *P<0.05 by Student-*t* test.

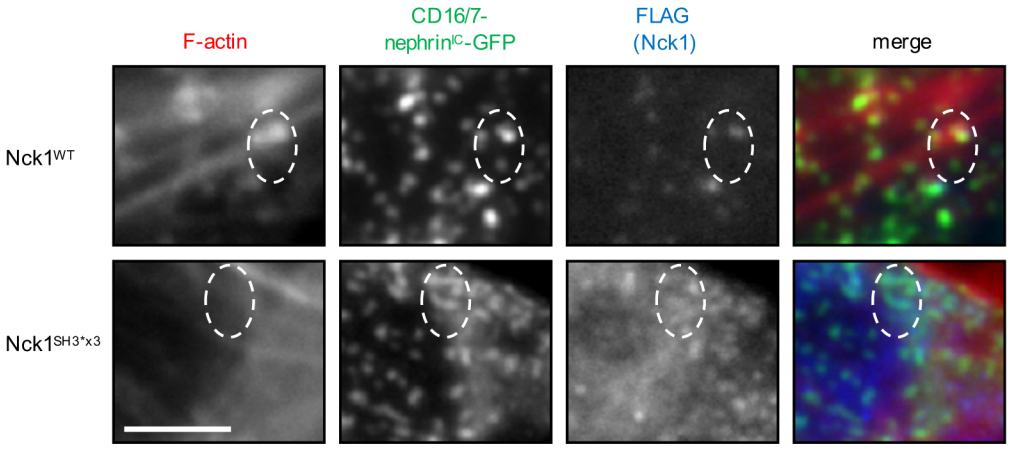

Figure S2. Nck1/2-null MEFs were co-transfected with CD16/7-nephrin(WT)^{IC}-GFP and FLAG-Nck1, stimulated with CD16 antibody, and immunostained as indicated. Mutation of the three Nck1 SH3 domains (SH3*x3) perturbs F-actin polymerization (red) compared to WT and induces a small amount of elongated clusters (green). Scale bar: 20 µm.

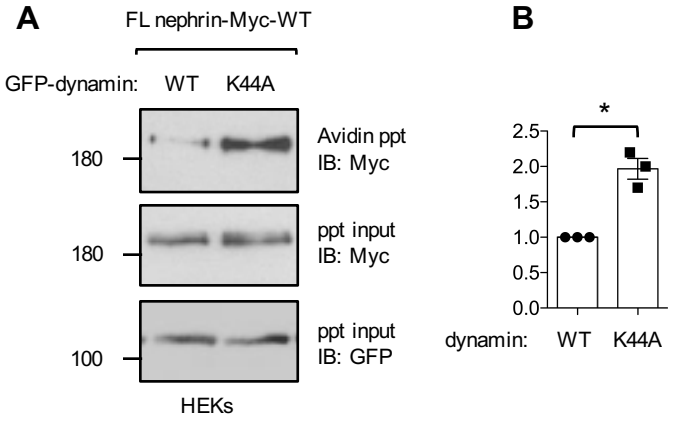

Figure S3. (A) Transfected HEK 293Ts with full-length nephrin-WT construct and either GFP-dynamin2-WT or K44A mutant were subjected to surface biotinylation, followed by lysis, streptavidin agarose precipitation (ppt) and immunoblotting (IB) as indicated. A portion of the initial lysate was saved to represent the input / total lysate. (B) Densitometric quantitation of surface/total nephrin from (A). Dynamin2-K44A values were made relative to dynamin2-WT (n=3). *P<0.05 by one-sample *t*-test.

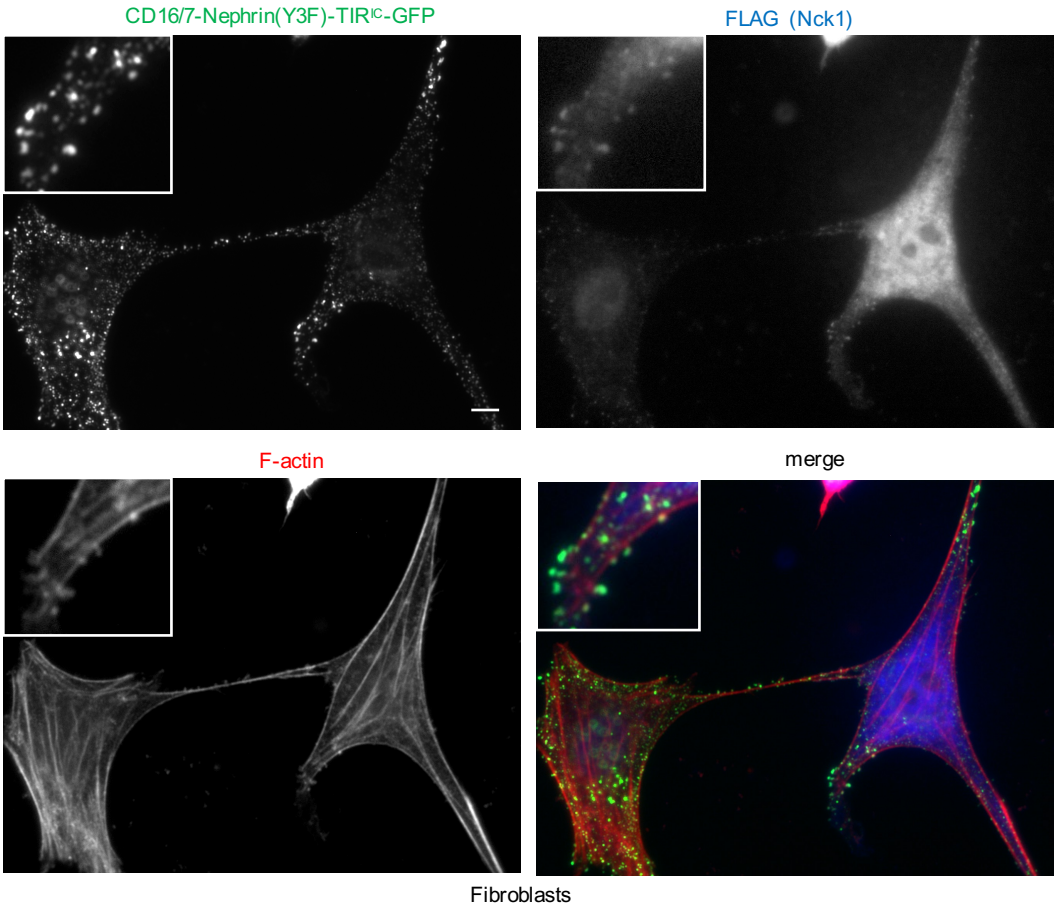

Figure S4. Addition of TIR sequence rescues CD16/7-nephrin(Y3F)^{IC}-GFP nephrin clustering in MEFs. Nck1/2-null MEFs were co-transfected with CD16/7-nephrin(Y3F)^{IC}-TIR-GFP and FLAG-Nck1, stimulated with CD16 antibody, and immunostained as indicated. Clustering of CD16/7-nephrin(Y3F)^{IC}-TIR-GFP results in Nck recruitment and restores normal punctate cluster morphology. Scale bar: 20 µm.